

Modeling AMP Degradation Product Formation

Christopher M. Parks,* Kevin J. Hughes, and Mohamed Pourkashanian



Cite This: *Ind. Eng. Chem. Res.* 2021, 60, 18337–18360



Read Online

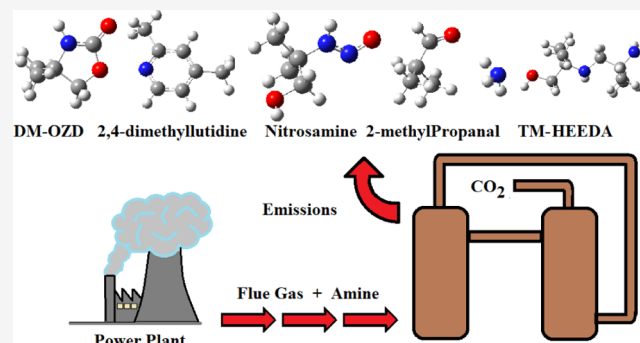
ACCESS |

Metrics & More

Article Recommendations

Supporting Information

ABSTRACT: A thorough understanding of the origin of all products arising from the degradation of amines used in carbon capture is crucial for the development of new and improved systems. Here, we present density functional theory (DFT) studies investigating the routes to thermal and oxidative degradation products of 2-amino-2-methyl-1-propanol (AMP). The formation of dimethyloxazolidinone (DMOZD) via the cyclization of carbamates, carbamic acids, and/or isocyanates is more favored for AMP than for monoethanolamine (MEA). In contrast, the formation of amides from the reaction of organic acids and AMP is unlikely due to large free activation energies. 2,4-Lutidine is predicted to form via the reaction of ammonia, propanone, and ethanal. Ammonia and low-molecular-weight organic acids are predicted to form favorably from AMP radical fragmentation. The network of elementary reactions investigated here can form the basis of a larger chemical kinetic model, which could be instrumental in predicting product formation in novel systems.



1. INTRODUCTION

Global temperatures have continued to rise over the last century. A rise that is, in part, attributed to the continued buildup of CO₂ in the atmosphere.¹ Electricity generation from a fossil-fuel-fired power station accounts for as much as a quarter of global CO₂ emissions: a number which in the short term is likely to rise. One of the most promising and widely studied technologies aiming to combat this buildup is amine-based postcombustion carbon capture.² This involves passing power station flue gas through an amine solution, where CO₂ binds to amine and can subsequently be removed and stored. This acts to reduce the amount of CO₂ that is expelled into the atmosphere.

To be considered suitable for this process, an amine must have good solubility, react rapidly and reversibly with CO₂, have good stability, and preferentially be economically viable. Currently, the industrial standard amine for this process is monoethanolamine (MEA), which meets many of these requirements. Despite this, MEA has a large energy penalty, which has been quoted to be as high as 10% of the total cost of the process.³ As a consequence, there is a drive to find a more viable amine for carbon capture.

To date, many amines have been investigated such as 2-amino-2-methyl-1-propanol (AMP), diethanolamine (DEA),^{4,5} ethylenediamine (EDA),^{6–8} methyldiethanolamine (MDEA),⁹ morpholine,^{10–12} and piperazine. Of these, AMP has shown promise as a solvent component in existing systems.^{13–19} It is more resistant to degradation, has higher absorption capacity,^{15,20} and requires less energy for regeneration.¹⁹ Its applicability is somewhat hindered, however, by poorer kinetics when compared to MEA.^{18,21} As a consequence, efforts have

been made to enhance the kinetics, for example, by doping the AMP solution with other amines.^{16,18}

Irrespective of the nature of the amine, solvent degradation remains a hindrance to the widespread use of this technology.³ Not only does this necessitate the replacement of a lost solvent, some of the degradation products can be harmful or toxic. Thermal degradation of the solvent occurs mainly in the stripper, where temperatures are generally higher than in the absorber to release the bound CO₂ from the amine. Oxidative degradation occurs mainly in the absorber where O₂ concentrations can reach 3–15%, dependent on the composition of the flue gas.^{22–24} It is considered to be radical driven, with the process initiated through either hydrogen or electron loss from the amine.

Figure 1 shows a selection of thermal and oxidative degradation products that have been characterized in various experimental studies on AMP degradation.^{25,26} These products are generally classified as primary, originating in reactions directly from the amine, or secondary, where primary products form under subsequent degradation reactions.

Clearly, a thorough understanding of the products formed during amine degradation is of paramount importance to the design of future systems. Moreover, rationalizing the specific

Received: October 4, 2021

Revised: November 30, 2021

Accepted: December 2, 2021

Published: December 13, 2021



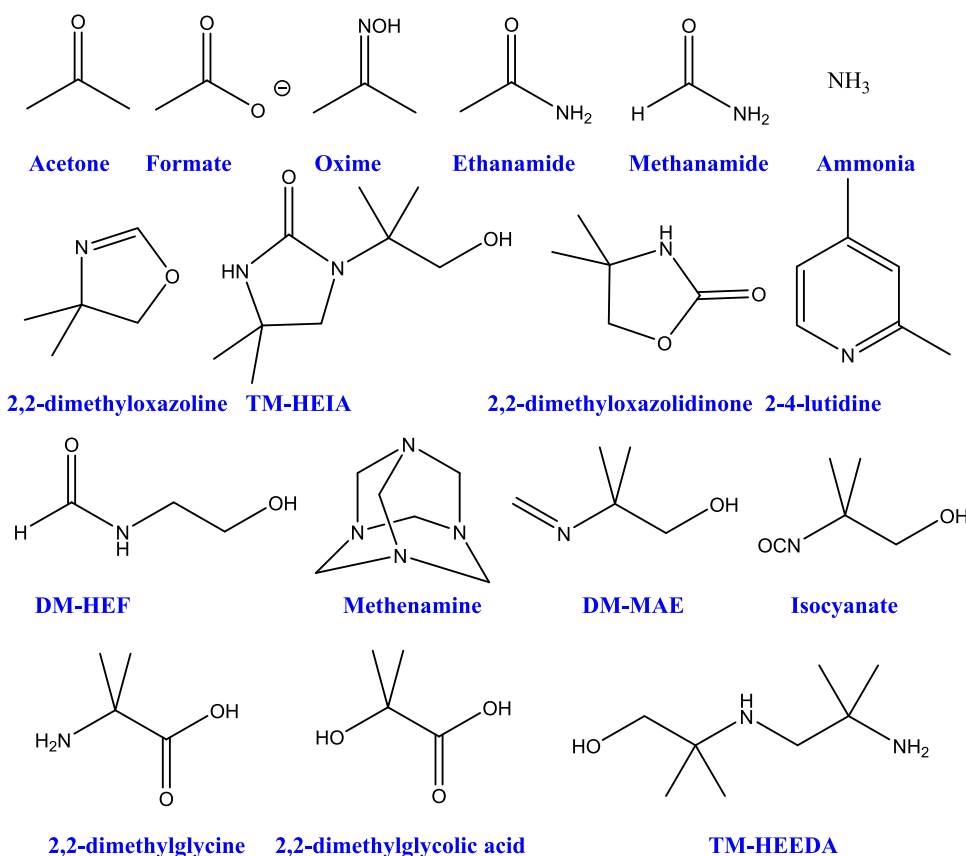
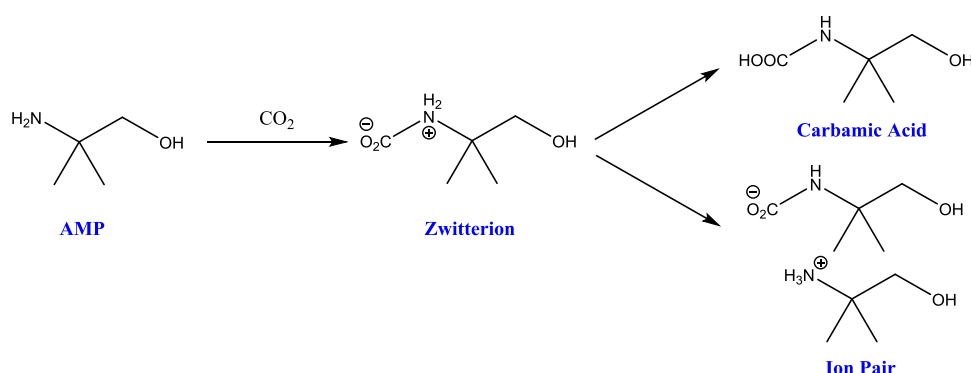


Figure 1. Major thermal and selected oxidative degeneration products of AMP.

Scheme 1. Reaction of AMP and CO₂ Leading to the Formation of Either an Ion Pair or Carbamic Acid



mechanisms which lead to those species might afford some insights into how to prevent the degradation.

Conducting such investigations is a challenging task; hence, molecular modeling can be employed to investigate reaction pathways in a timely manner. While the number of computational investigations remains low in comparison to experimental, several studies have nevertheless been conducted. Several degradation products of MEA were investigated by Vevelstad et al. using quantum mechanics and predicted to form favorably.²⁷ The formation of imidazolidinone from MEA was modeled by Saeed and co-workers.²⁸ More recently, Yoon et al. reported more detailed first-principles studies on the thermal degradation of MEA.²⁹ The differing mechanisms of CO₂ reacting with MEA and AMP were investigated by Xie et al.³⁰ Further studies have focused on the initial binding of amines and CO₂.^{31–33}

Each of these studies focuses on a small number of reactions involved in amine degradation. In this paper, we use density functional theory (DFT) to more widely investigate the chemical pathways involved in AMP degradation. The calculated activation energies are scrutinized to assess which pathways and products are most likely. Comparisons are made with experimental observations.

2. COMPUTATIONAL DETAILS

DFT calculations were performed using Gaussian 09 software, version D.01,³⁴ using Gaussian-supplied versions of BLAS and ATLAS.³⁵ All calculations used the B3LYP functional,^{33,36} and the cc-pVTZ basis set was used for all elements.³⁷ This setup was chosen to be consistent with previously published work within the group and to allow for comparisons with that work.³⁸ Moreover, benchmarking studies have shown this setup to be

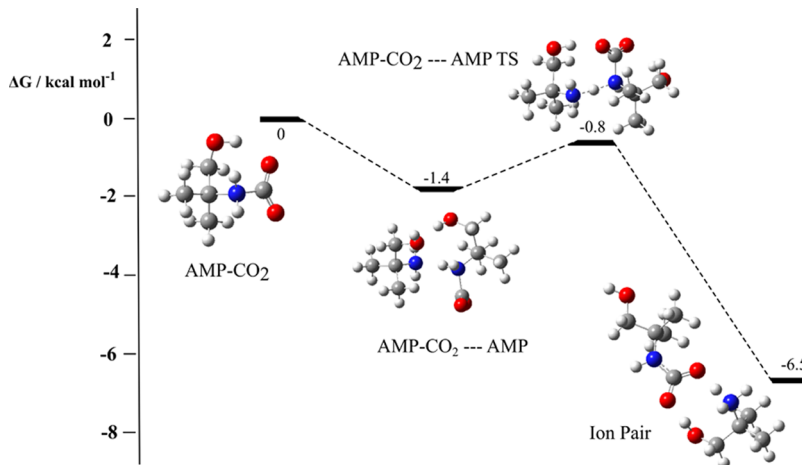


Figure 2. DFT-calculated free-energy profile for the proposed formation of an ion pair from AMP-CO₂.

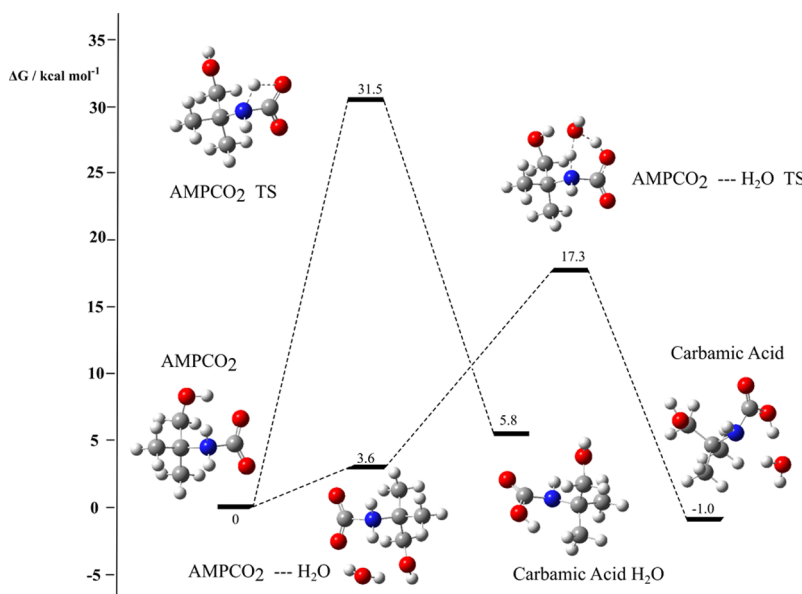
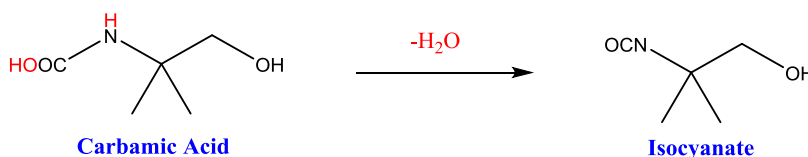


Figure 3. DFT-calculated free-energy profile for the proposed formation of carbamic acid from AMP-CO₂.

Scheme 2. Formation of Isocyanate from Carbamic Acid



similar in quality to that afforded by CCSD(T) calculations and can be conducted in a more timely manner.^{39,40} Calculations were carried out at 298.15 K. Empirical dispersion corrections through the GD3 keyword were applied to all calculations. In all calculations, the solvent was accounted for by the polarizable continuum model (PCM) method using solvent parameters for water as implemented in Gaussian.^{41,42} Geometry optimizations were confirmed to be local minima by the absence of imaginary frequencies in the vibrational spectra. Transition states were optimized using the QST3 method as implemented in Gaussian.⁴² All transition states were confirmed both visually via the presence of one large imaginary frequency corresponding to the saddle point and via intrinsic reaction coordinate (IRC) scans. An ultrafine grid was employed for all calculations with no

symmetry constraints. Radical species were calculated as singlets with the highest occupied molecular orbital (HOMO) and lowest unoccupied molecular orbital (LUMO) orbitals mixed (guess = mix option) to break the symmetry of the system unless stated otherwise. Free energies were calculated using the Grimme quasiharmonic entropy correction using the Good-Vibes script.⁴³ Activation energies are calculated as the energy difference between the transition state and both reactants at infinite separation.

3. RESULTS

3.1. Thermal Degradation. 3.1.1. Formation of Carboxylates, Carbamic Acid, and Ion Pair. The first products observed during AMP carbon capture originate from the

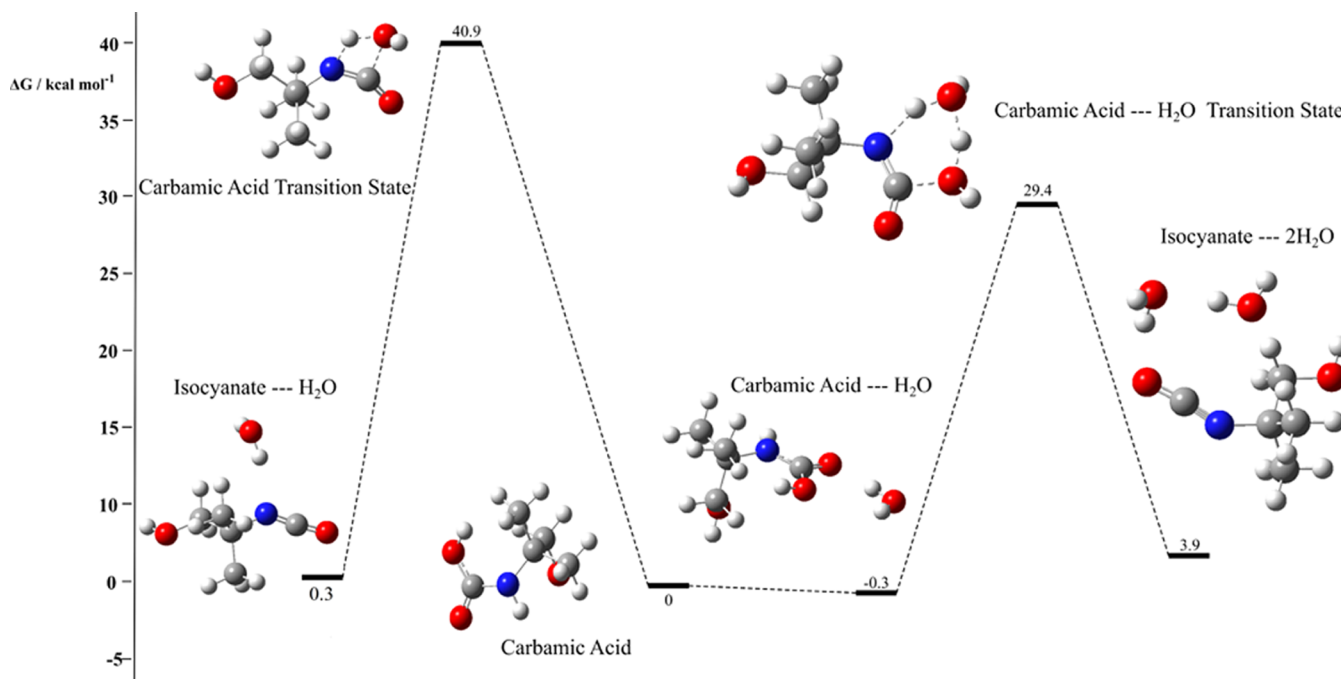


Figure 4. DFT-calculated free-energy profile for the proposed formation of isocyanate *via* two alternative routes.

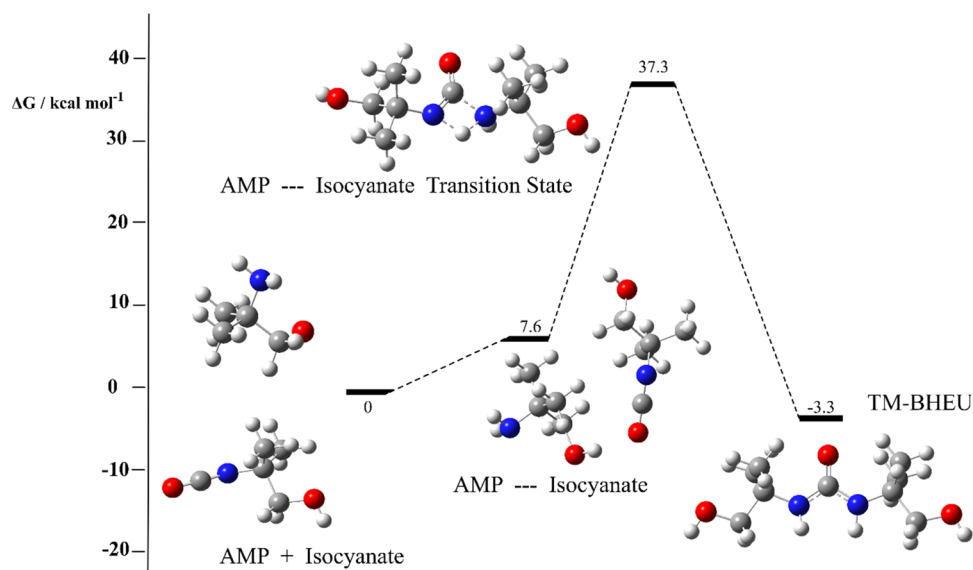


Figure 5. DFT-calculated free-energy profile for the proposed formation of TM-BHEU from the reaction of AMP and isocyanate.

reactions of CO₂ and the nitrogen atom of the amine. As shown in **Scheme 1**, the binding of CO₂ to the amine leads to a zwitterionic complex containing a positively charged nitrogen and negatively charged oxygen. The zwitterion can undergo a hydrogen transfer reaction to form a carbamic acid. Alternatively, it can react with a further molecule of AMP to form an ion pair. Should the formation of the ion pair be the dominant reaction, it would lead to a CO₂ loading of 0.5 compared to AMP. The calculated free-energy profiles for the formation of the ion pair and carbamic acid are shown in **Figures 2** and **3**, respectively.

In **Figure 2**, the prereaction complex, defined as the structure immediately preceding the transition state with the two reactants in close proximity (AMP–CO₂···AMP) is more stable than the separated reactants. This is attributed to hydrogen

bonding between the reactants. The oxygen–hydrogen distance is 1.83 Å and the nitrogen–hydrogen distance is 1.80 Å. This complex is perfectly orientated to allow for hydrogen transfer from the zwitterion nitrogen to the other AMP molecule. The free activation energy is very low (0.6 kcal mol⁻¹), which is consistent with recently reported data for MEA (1.2 kcal mol⁻¹).³⁸ The reaction energy is also exergonic at −6.5 kcal mol⁻¹, suggesting that the formation of an ion pair should be relatively facile.

Figure 3 shows two routes to the formation of carbamic acid, one resulting from an isolated AMP–CO₂ and a further route facilitated by the presence of an explicit water molecule. The activation free energy for the water-assisted pathway is significantly lower than the unimolecular reaction (17.3 *cf.* 31.5 kcal mol⁻¹). Due to the computational cost of explicitly

Scheme 3. Routes to the Formation of Bicarbonate

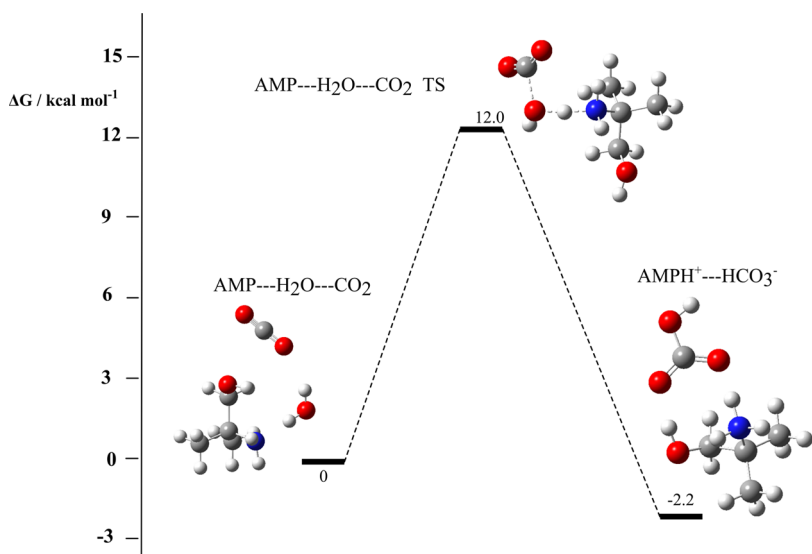
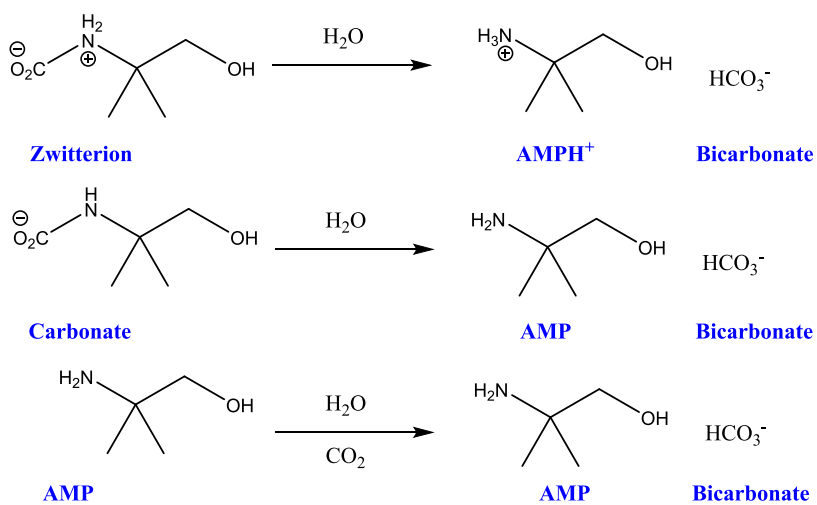


Figure 6. DFT-calculated free-energy profile for the proposed formation of bicarbonate from free CO₂, H₂O, and AMP.

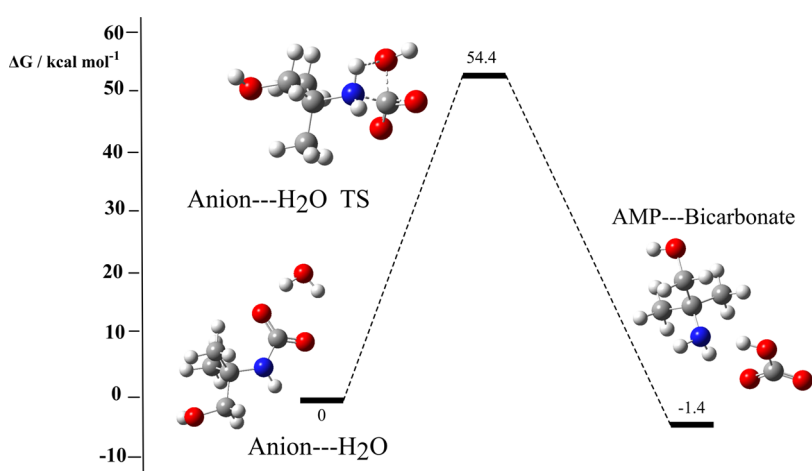


Figure 7. DFT-calculated free-energy profile for the proposed formation of bicarbonate.

including solvent molecules, this methodology cannot be applied to each reaction. However, it does highlight the importance of the solvent environment in accurately predicting

reaction barriers. While the formation of carbamic acid is less favorable than the formation of an ion pair, it could still become a relevant reaction if the CO₂ loading is high enough. In this

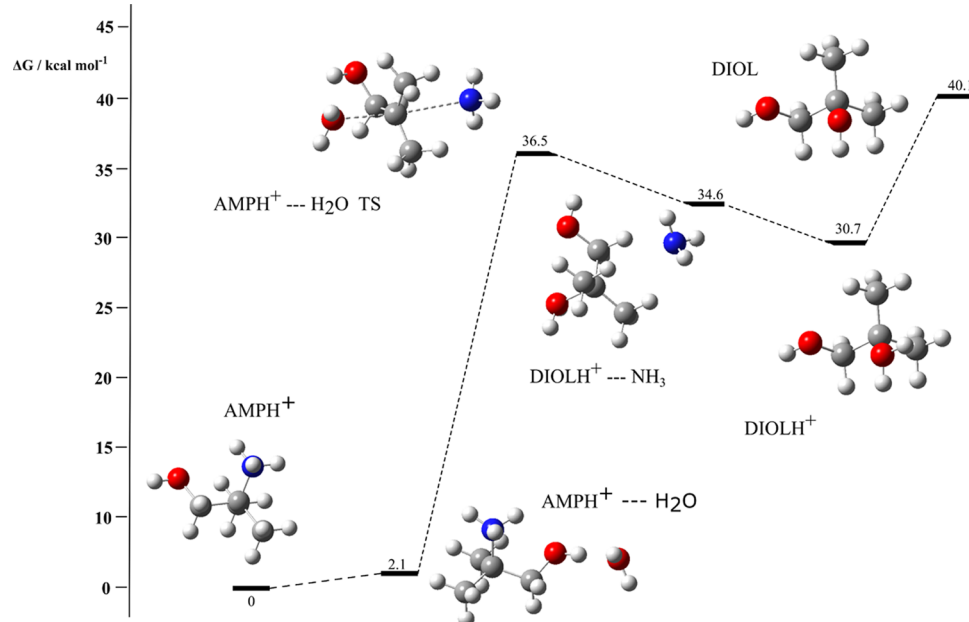
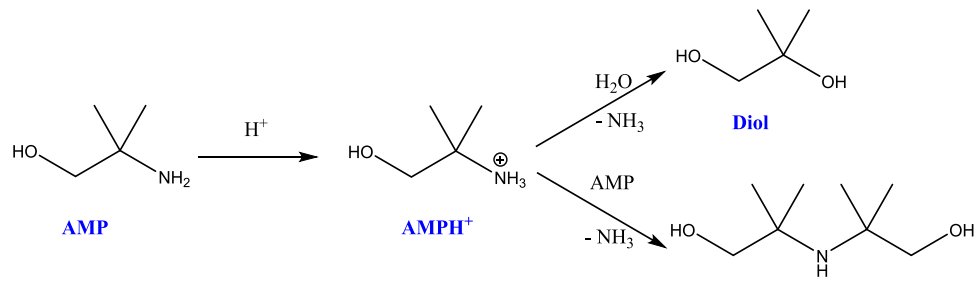
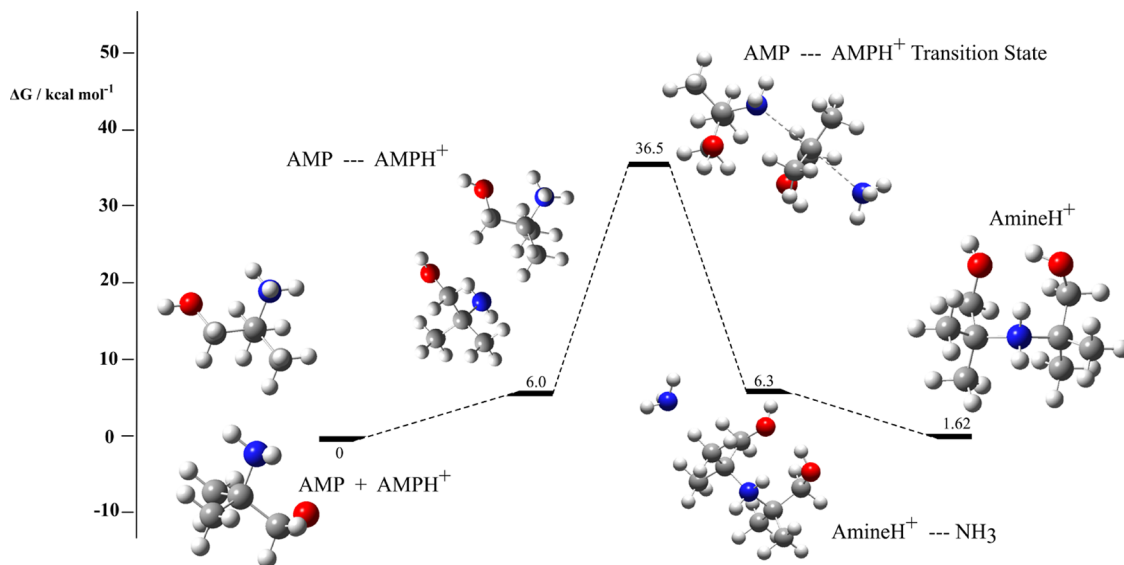
Scheme 4. Reactions of Protonated AMP with H₂O or AMP

Figure 8. DFT-calculated free-energy profile for the proposed formation of a diol from AMP.

Figure 9. DFT-calculated free-energy profile for the proposed formation of TM-DEA from AMP and AMPH⁺.

situation, the concentration of AMP-CO₂ would greatly exceed that of free AMP, and thus the formation of carbamic acid would be favored.

If any carbamic acid were to form, there are a number of reactions that could subsequently undergo. For example, the

transformation of carbamic acids into isocyanates has been observed experimentally.^{44,45} The reaction is summarized in Scheme 2 and was subsequently investigated here. Figure 4 shows the DFT-calculated free-energy profile for isocyanate formation from carbamic acid. In this case, two distinct pathways

Scheme 5. Two Routes to the Formation of DMOZD

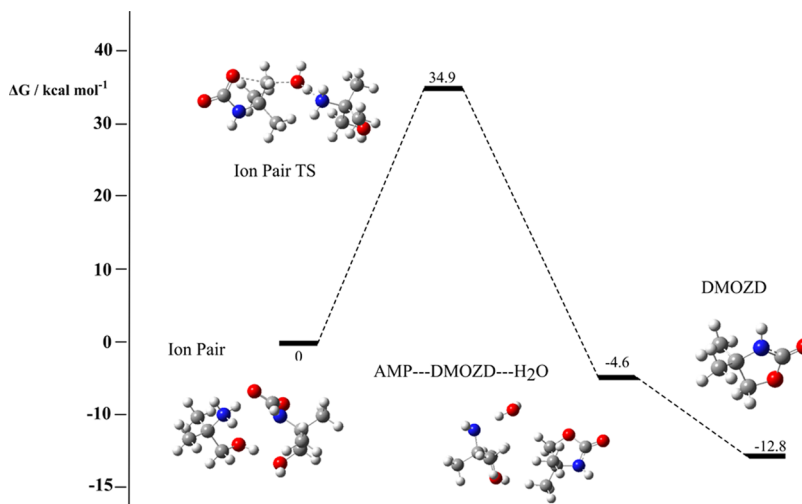
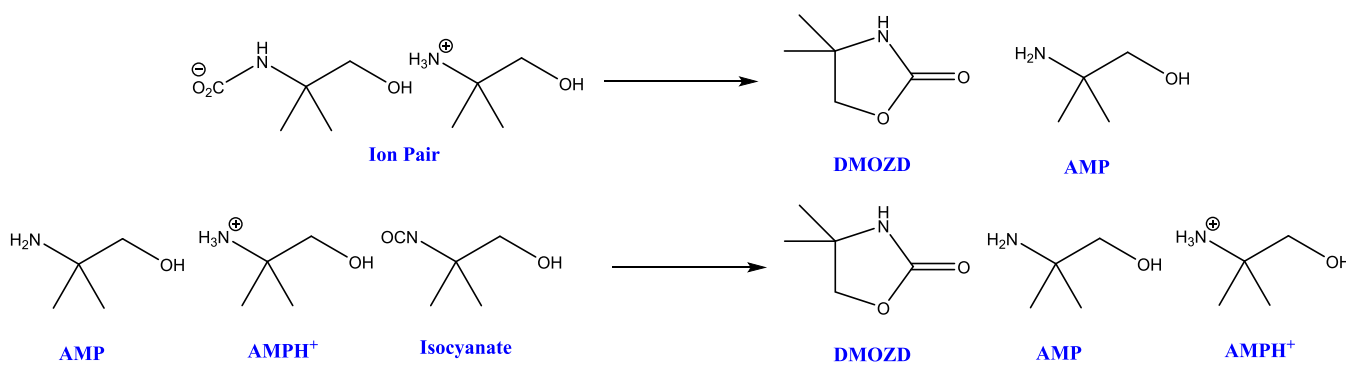


Figure 10. DFT-calculated free-energy profile for the proposed formation of DMOZD from an ion pair.

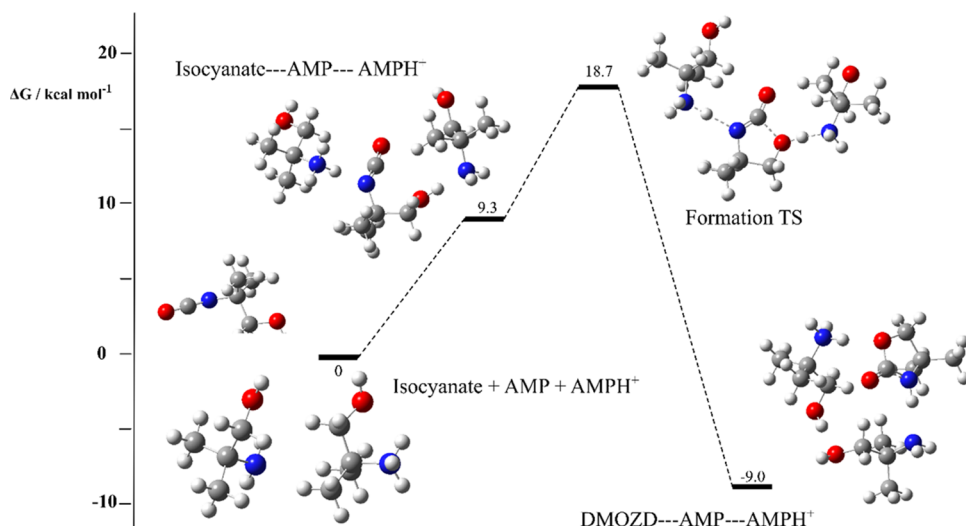
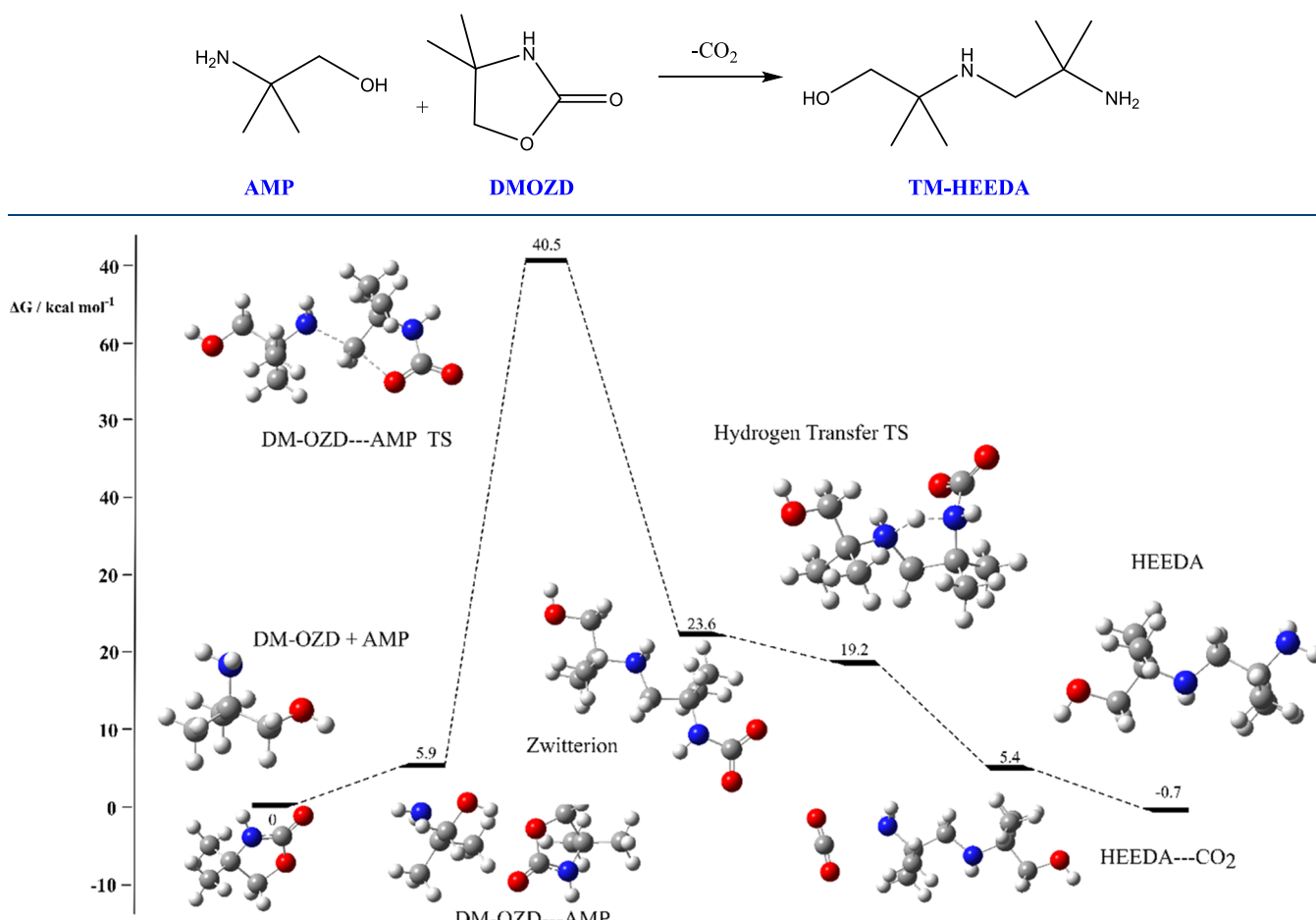
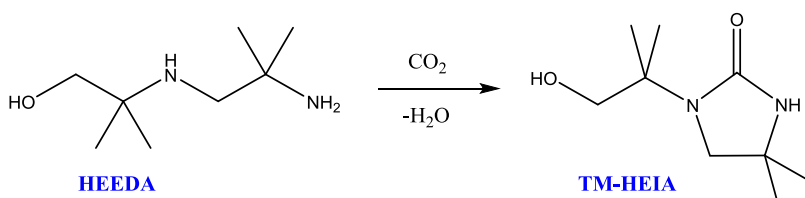


Figure 11. DFT-calculated free-energy profile for the proposed formation of DMOZD from isocyanate.

were again located, one with and one without an explicit water molecule. In the intramolecular reaction, OH from the $-\text{CO}_2\text{H}$ motif and a hydrogen bound to the nitrogen are eliminated to form isocyanate. In the water-facilitated reaction, the hydrogen bound to the amine is transferred to the water molecule. Concurrently, water protonates the OH of the $-\text{CO}_2\text{H}$ group, which eliminates water and forms the isocyanate. This reaction has a lower activation free energy than the intramolecular

reaction. For both modeled pathways in Figure 4, the reaction is endergonic, which is consistent with reported literature data for MEA²⁹ and AMP⁴⁶ that also predict carbamic acid to be more stable than isocyanate.

Isocyanates are susceptible to nucleophilic attack. Given that AMP is likely to be the most prevalent amine in the system, the reaction of AMP and isocyanate was probed. Figure 5 shows the free-energy profile for the formation of a methyl-substituted

Scheme 6. Proposed Formation of TM-HEEDA from AMP and DMOZD**Figure 12.** DFT-calculated free-energy profile for the proposed formation of TM-HEEDA from DMOZD and AMP.**Scheme 7.** Proposed Formation of HEIA from TM-HEEDA and CO₂

variant of *N,N'*-bis-(2-hydroxyethyl)urea (BHEU), *N,N'*-bis(2-hydroxy-1,1-dimethylethyl)urea (TM-BHEU). The nucleophilic nitrogen on AMP attacks the isocyanate carbon atom. Hydrogen transfer between the two nitrogen atoms leads to the formation of the target compound. The reaction is overall exergonic.

The formation of bicarbonate has been observed in experimental AMP systems, more so than in MEA systems. Bicarbonate could be formed from zwitterion, carbamic acid, carbonate anion, or from free AMP, H₂O, and CO₂ in a ternary reaction as summarized in **Scheme 3**. In the latter, CO₂ is not bound to AMP but is in close proximity. The nitrogen atom of AMP acts as a nucleophile and abstracts a proton from water. Concurrently, the liberated hydroxide attacks the carbon atom in CO₂ to form bicarbonate. The free-energy profile for this reaction is shown in **Figure 6**. As can be seen, the reaction has low free activation energy and is overall exergonic, suggesting

that bicarbonate could form easily *via* this route. The only limitation to this reaction is the three reactants coming together in the correct orientation for a reaction to occur.

In contrast, **Figure 7** shows that the formation of bicarbonate *via* water attacking an anion complex is prohibited by a very large free activation energy. This is consistent with other literature studies that also predict a large barrier for this conversion.

3.1.2. Protonation Products. We recently reported on the degradation reactions of piperazine during carbon capture. Protonation of the amine group was found to be a critical step in the formation of many degradation products.⁴⁷ Similar protonation of the amine group in AMP might facilitate reactions with other amines and/or water, as shown in **Scheme 4**. This leads to the formation of TM-DEA or a diol, respectively.

The free-energy profile for the formation of a diol from the reaction of AMPH⁺ and water is shown in **Figure 8**. As can be seen, the reaction has a relatively high free activation energy and

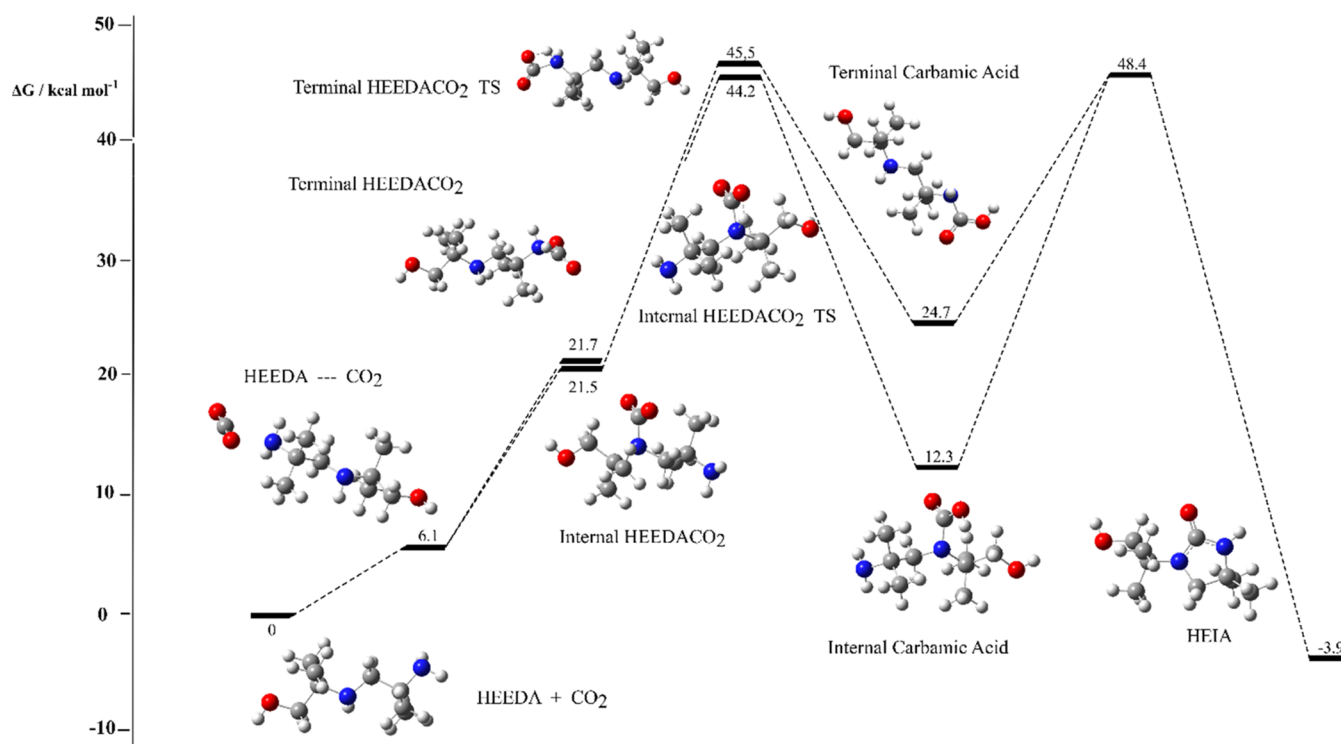


Figure 13. DFT-calculated free-energy profile for the proposed formation of TM-HEIA from TM-HEEDA and CO₂.

Scheme 8. Proposed Formation of 1,3-di-(1,1-dimethyl-2-Hydroxyethyl)-4,4-dimethyl-2-imidazolidinone (TM-AHEIA) from TM-HEEDA and DMOZD

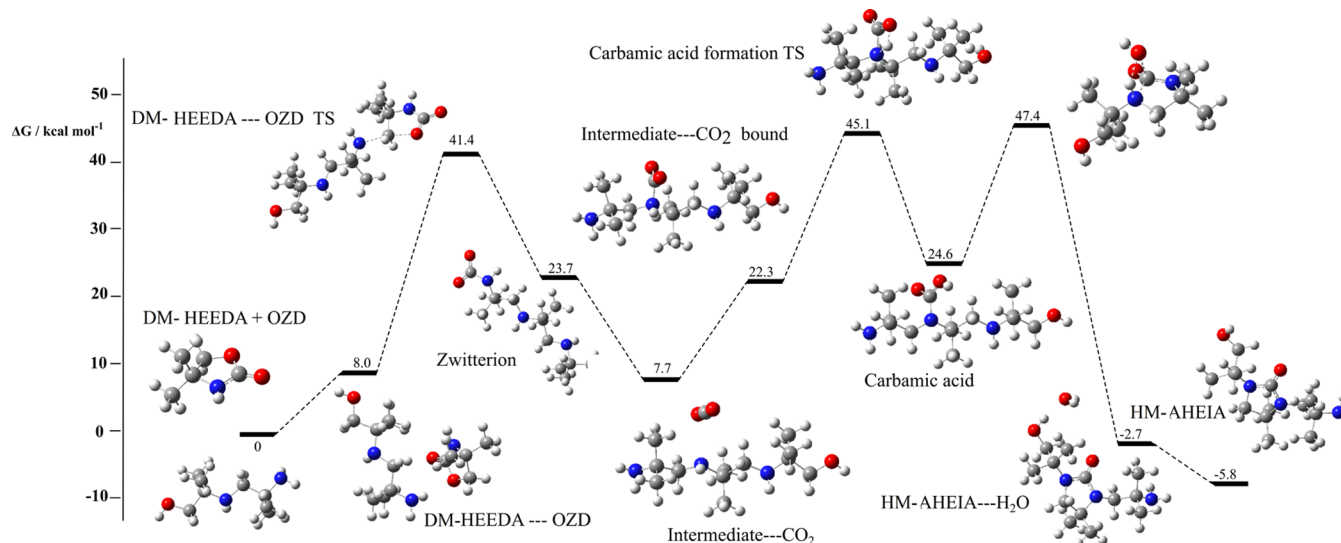
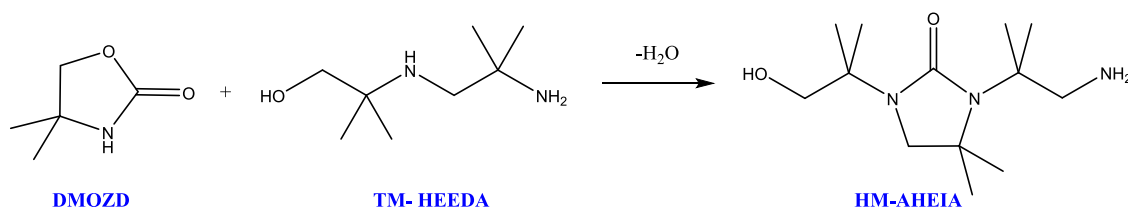
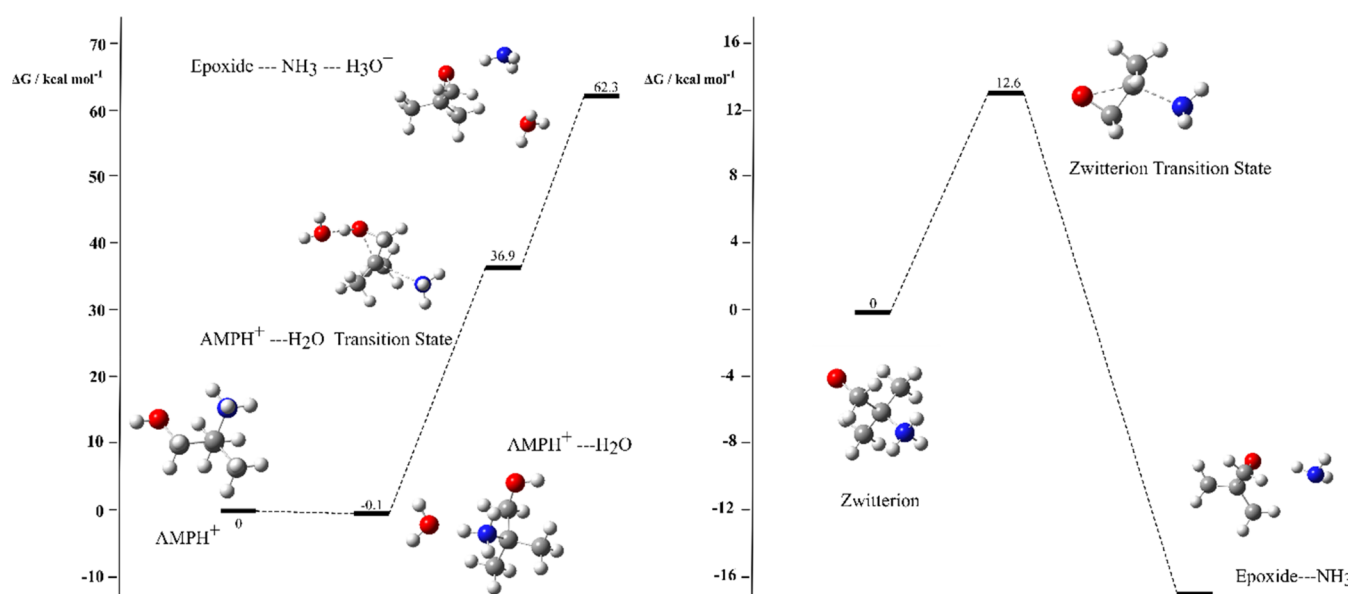
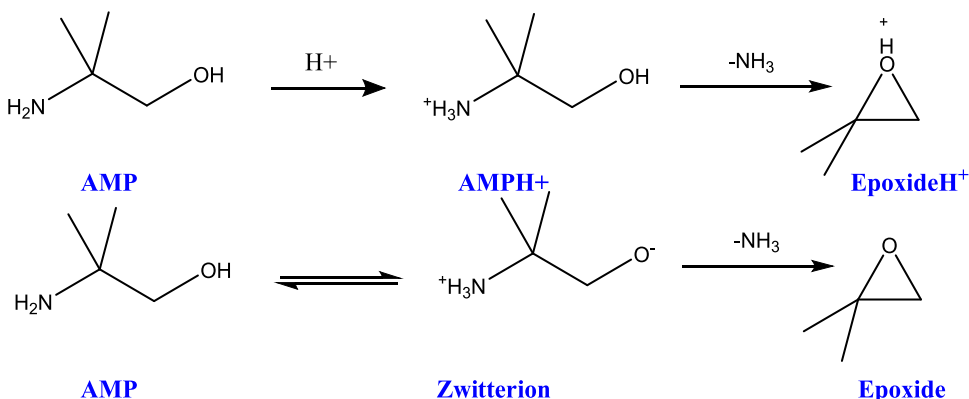


Figure 14. DFT-calculated free-energy profile for the proposed formation of HM-AHEIA from DMOZD and AMP.

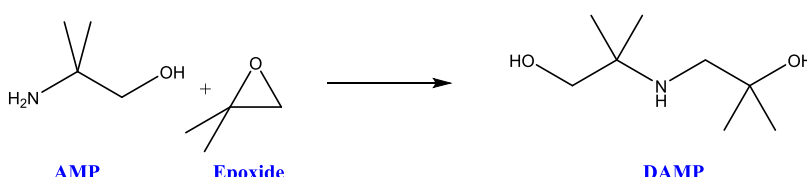
is overall endergonic. Similar results were recently reported for MEA.³⁸ While the formation of the diol is not strictly prohibited, its formation is unlikely. Any diol formed would be susceptible

to nucleophilic substitution; this reaction would have low free activation energy and be strongly exergonic.

Scheme 9. Two Potential Routes to the Formation of Epoxides and Ammonia from AMP

Figure 15. DFT-calculated free-energy profiles for the proposed formation of epoxides from AMPH⁺ (left) and a zwitterion (right).

Scheme 10. Potential Formation of DAMP from AMP and an Epoxide



In contrast, the reaction of AMP and AMPH⁺ is much more likely. The free-energy profile in Figure 9 shows that the reaction has similar free activation energy compared to the hydrolysis reaction in Figure 8. However, the reaction is only marginally endergonic (1.6 kcal mol⁻¹) and could easily be surmounted given standard experimental conditions experienced in carbon capture systems.

3.1.3. Formation of Dimethyloxazolidinone (DMOZD). Oxazolidinone (OZD) is an important intermediate in MEA degradation and is a precursor to the formation of *N*-(2-hydroxyethyl)ethylenediamine (HEEDA), *N*-(2-aminoethyl)-*N'*-(2-hydroxyethyl)imidazolidin-2-one (HEIA), and *N*-(2-aminoethyl)-*N'*-(2-hydroxyethyl)imidazolidin-2-one (AHEIA).^{45,48} Degradation of AMP can form a substituted analogue of OZD, 4,4-dimethyl-2-oxazolidinone (DMOZD).

Two routes to its formation are shown in Scheme 5. Isocyanate can cyclize to form the target complex, facilitated by AMP and AMPH⁺, which are necessary to carry out the transfer of hydrogens. Alternatively, an ion pair species can lead to the formation of DMOZD and AMP.

Figure 10 presents the DFT-calculated free-energy profile for the formation of DMOZD from an ion pair. In the transition state, a five-membered ring is formed when the carboxylate oxygen attacks the carbon atom α to the hydroxyl group. The cationic AMPH⁺ provides a hydrogen, which reacts with the hydroxide leaving group and forms water. Overall, this reaction forms DMOZD, water, and AMP. The activation free energy is 34.9 kcal mol⁻¹, which is lower than the recently reported value for OZD formation in MEA degradation (39.3 kcal mol⁻¹) and is consistent with a more nucleophilic amine.³⁸

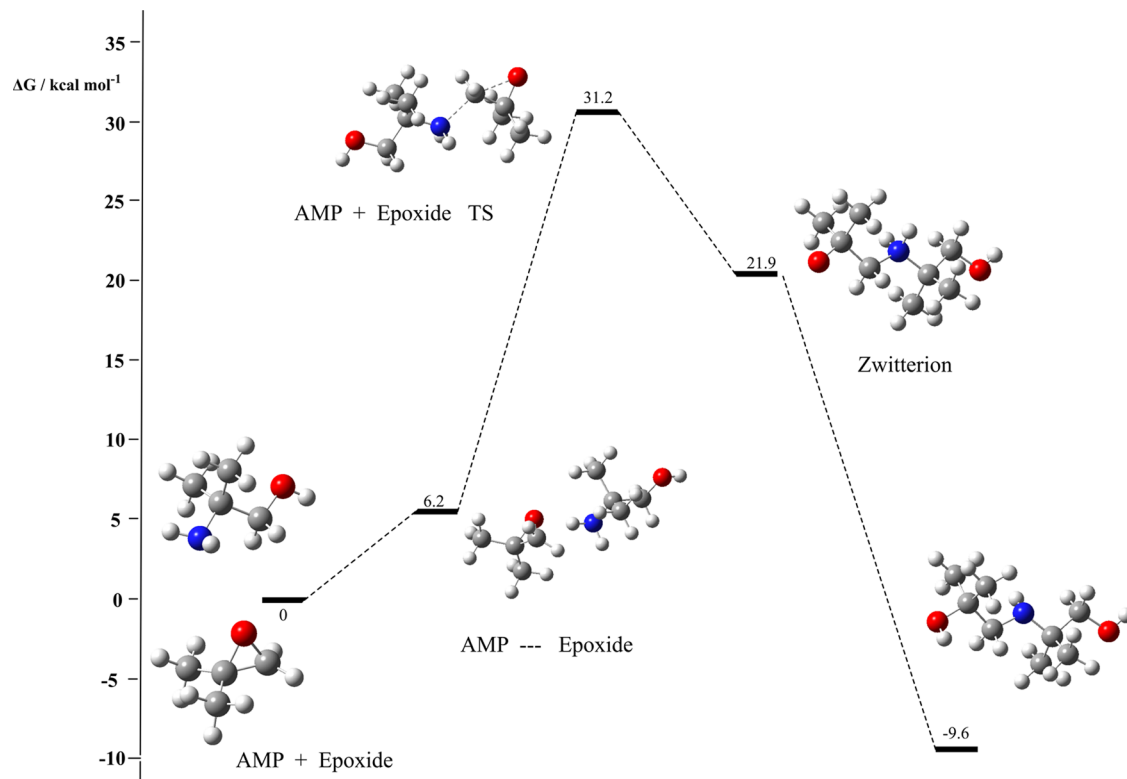


Figure 16. DFT-calculated free-energy profile for the proposed formation of DAMP from AMP and epoxide.

Scheme 11. Proposed Formation of DM-MAE from AMP and Formaldehyde

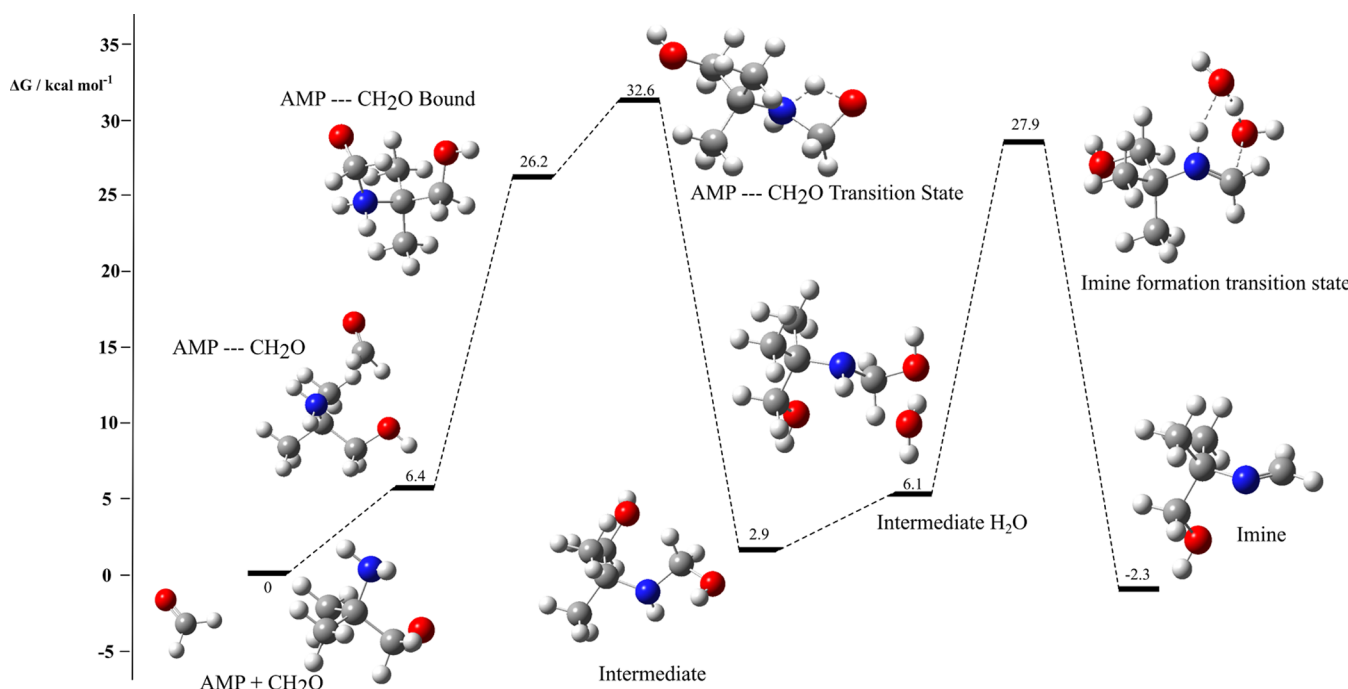
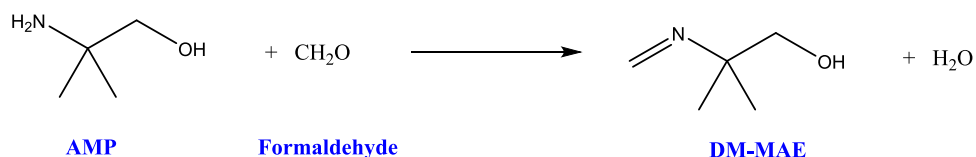


Figure 17. DFT-calculated free-energy profile for the proposed formation of DM-MAE from AMP and formaldehyde.

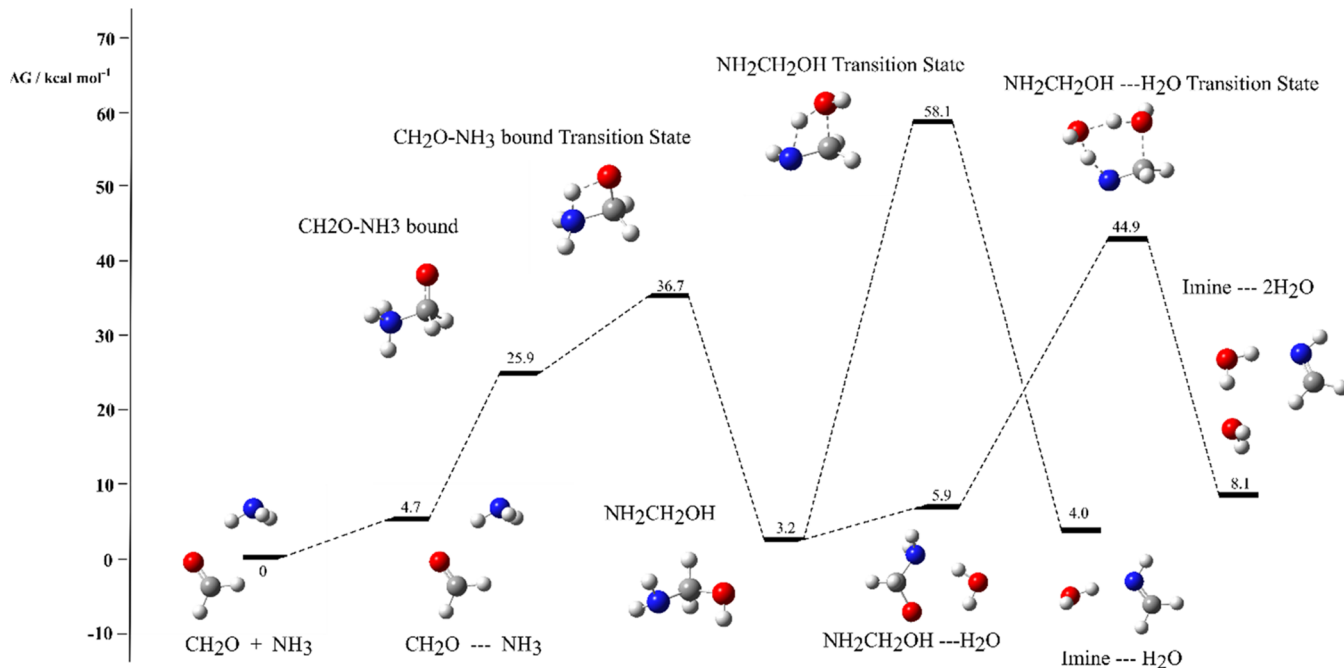


Figure 18. DFT-calculated free-energy profile for the proposed formation of an imine.

Scheme 12. Formation of Nitrosamines and Nitramines from AMP

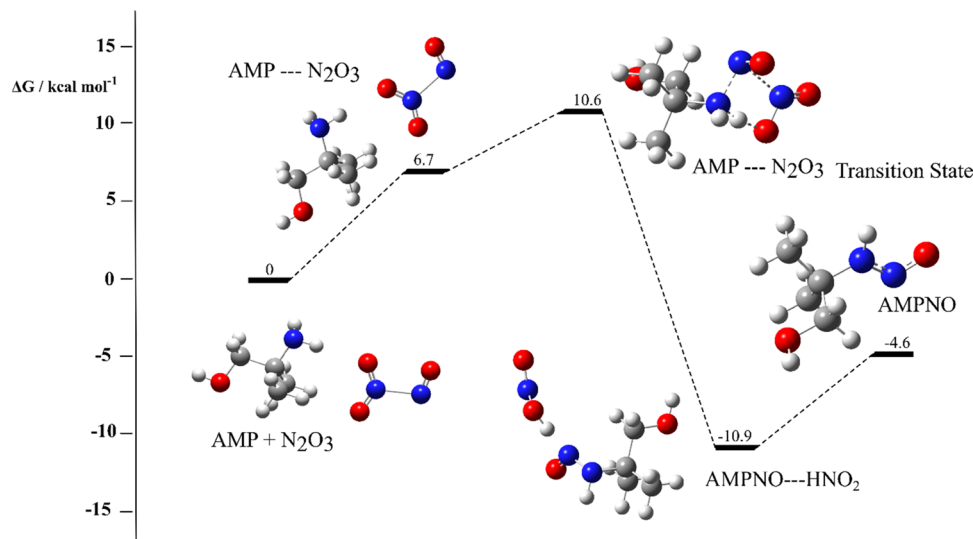
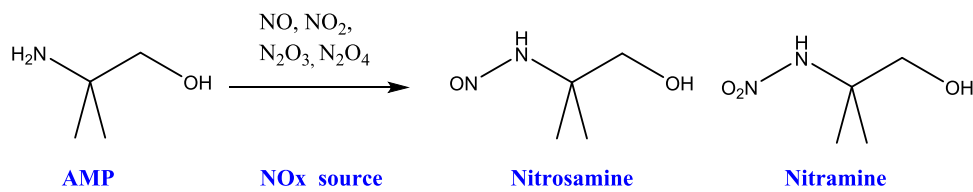


Figure 19. DFT-calculated free-energy profile for the formation of a nitrosamine from AMP and N₂O₃.

Figure 11 shows the free-energy profile for the formation of DMOZD from isocyanate. Here, hydroxyl oxygen acts as a nucleophile and attacks the carbon of the isocyanate group. AMP acts as a nucleophile and deprotonates the hydroxyl group, and the protonated AMP provides a proton for the isocyanate group. The free activation energy for this reaction is 18.7 kcal mol⁻¹, and the reaction is overall exergonic. This suggests that any isocyanate present could easily convert into DMOZD. This

reaction would be much more favored than the formation of BHEU presented earlier, which has a much larger free activation energy.

3.1.4. Formation of 2-[(2-Amino-2-methylpropyl)amino]-2-methyl-1-propanol (TM-HEEDA), 1-(1,1-dimethyl-2-Hydroxyethyl)-4,4-dimethyl-2-imidazolidinone (TM-HEIA), and HM-AHEIA. HEEDA is formed in MEA degradation after the formation of OZD but before the formation of HEIA or AHEIA.

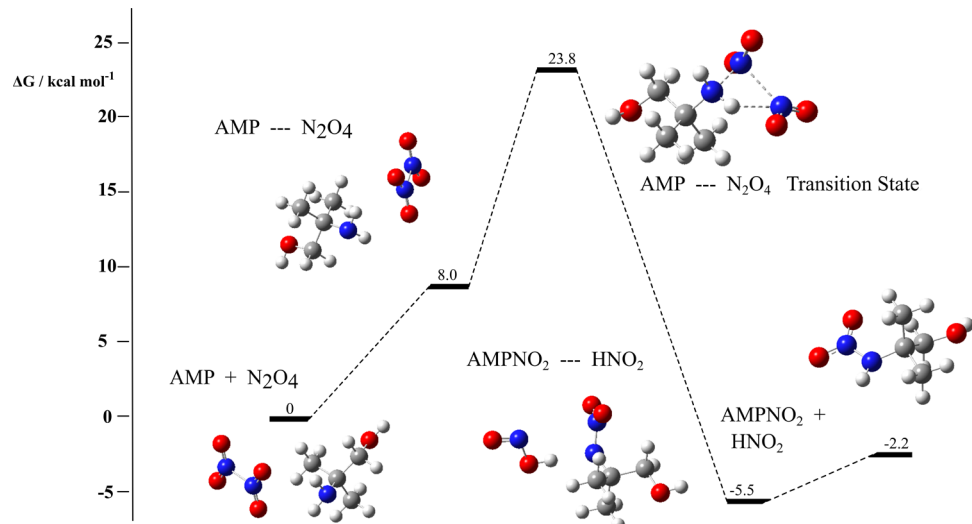


Figure 20. DFT-calculated free-energy profile for the formation of a nitramine from AMP and N_2O_4 .

Table 1. Activation Free Energies for the Formation of Nitrosamines and Nitramines from the Reaction of N_2O_3 and N_2O_4 with Various Primary and Secondary Amines

Molecule	Reactive site	ΔG free activation energy / kcal mol ⁻¹	
		Nitrosamine formation	Nitramine formation
TM-HEIA		22.7	36.3
DMOZD		25.7	43.1
TM-HEEDA		16.6 11.3	24.0

With a similar structure, it is likely that AMP degradation follows a similar path so this was investigated next. A methyl-substituted variant, TM-HEEDA, can form from the reaction of AMP and DMOZD according to Scheme 6. The free-energy profile is shown in Figure 12. Initially, nucleophilic attack of the AMP nitrogen atom on the CH_2 linker of DMOZD causes the ring to open and results in a zwitterionic species. This has an activation free energy of 40.5 kcal mol⁻¹. Hydrogen transfer from the protonated amine to the terminal amine facilitates the loss of CO_2 from the terminal amine and generates the target molecule TM-HEEDA.

Once successfully formed, TM-HEEDA can react with CO_2 to form TM-HEIA (a substituted version of HEIA) according to Scheme 7. There are two amine groups present in TM-HEEDA, either of which can bind with CO_2 . As shown in Figure 13, our calculations show that there is little preference as to which site CO_2 binds (the energies differ by 0.2 kcal mol⁻¹). The zwitterionic species in each case can undergo a 1,3-H-transfer reaction to form a carbamic acid. The activation free energies are 44.2 and 45.5 kcal mol⁻¹ when compared to the separated

reactants. This energy can likely be lowered with the inclusion of explicit water molecules as demonstrated previously. Either of the carbamic acids can cyclize with the elimination of water to form TM-HEIA, which is calculated to be 3.9 kcal mol⁻¹ more stable than the separated reactants.

A further reaction that TM-HEEDA can undergo is with DMOZD. This forms HM-AHEIA according to Scheme 8. Initially, the terminal amine on TM-HEEDA acts as a nucleophile and attacks the CH_2 linker on the ring of DMOZD. This causes the ring to open and forms a zwitterion complex. Figure 14 shows this step to have an activation free energy of 41.4 kcal mol⁻¹. To form HM-AHEIA, CO_2 needs to bind to one of the internal nitrogen atoms. Once appropriately bound, the carbonate can undergo a 1,3-hydrogen transfer reaction (or an intermolecular reaction where water facilitates the transfer) to form a carbamic acid. Lastly, a ring formation reaction can occur, which eliminates water and forms the target complex. While the reaction is exoergic overall, the relatively high barriers and number of required steps would suggest that HM-AHEIA forms slowly and in low quantity.

Scheme 13. Alternative Route to the Formation of TM-HEEDA

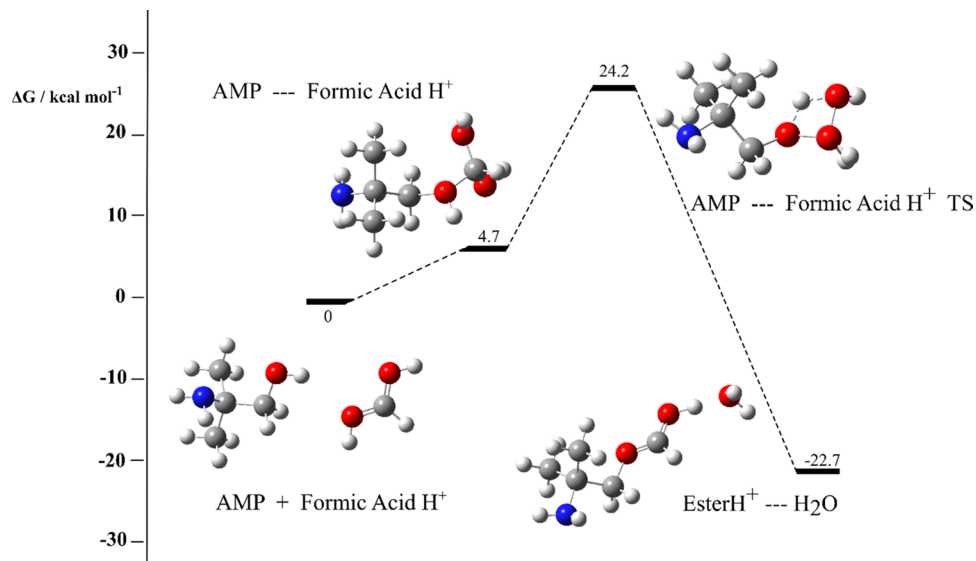
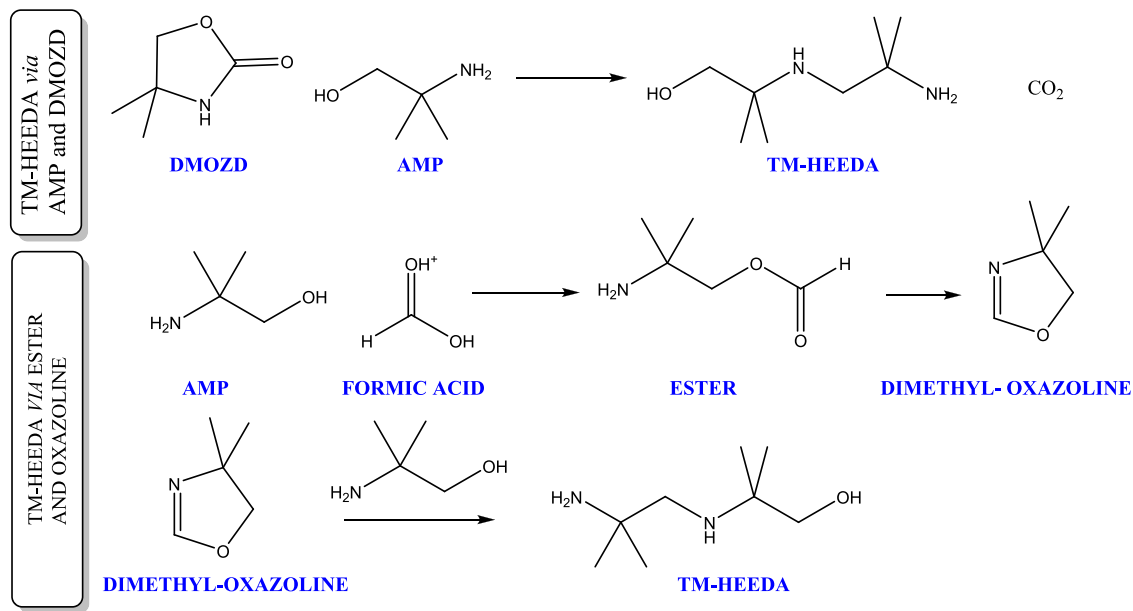


Figure 21. DFT-calculated free-energy profile for the formation of an ester from AMP and formic acid.

3.1.5. Formation of Epoxides. The formation of epoxides during MEA degradation has been suggested by Lepaumier.⁴⁹ If they do form, it could potentially open up new routes to products that would otherwise be difficult to rationalize. Two potential routes to the formation of epoxides from AMP are shown in Scheme 9. Prior protonation of amine nitrogen can create a better leaving group (NH_3^+ compared to NH_2^-) and could facilitate the nucleophilic substitution reaction to form an epoxide. Alternatively, an epoxide could form from a zwitterion form of AMP.

Both of these potential routes were investigated and free-energy profiles are shown in Figure 15. The formation of an epoxide from protonated AMP is unlikely. The activation energy is high, and the reaction is overall highly endergonic. On the other hand, formation from a zwitterion is possible given standard experimental conditions. It has a low free activation energy (12.6 kcal mol⁻¹), and the reaction is exergonic overall. It

is noted, however, that the zwitterion must first form from AMP if this reaction is to proceed, which would carry its own energy penalty.

Epoxides are susceptible to nucleophilic attack due to the strained nature of the three-membered ring. This ring strain can be relieved by attack at a carbon α to the oxygen atom. The most abundant nucleophile present in the reaction mixture is likely to be AMP, which is investigated here as a model reaction. Scheme 10 details the reaction to form 2-[(2-hydroxy-2-methylpropyl)-amino]-2-methyl-1-propanol (DAMP).

Figure 16 shows the free-energy profile for the reaction. The free activation energy for the nucleophilic attack is 31.2 kcal mol⁻¹. The free reaction energy is also exergonic (-9.6 kcal mol⁻¹). Both of these observations suggest a facile reaction, consistent with relieving the strain of the three-membered ring in the epoxide.

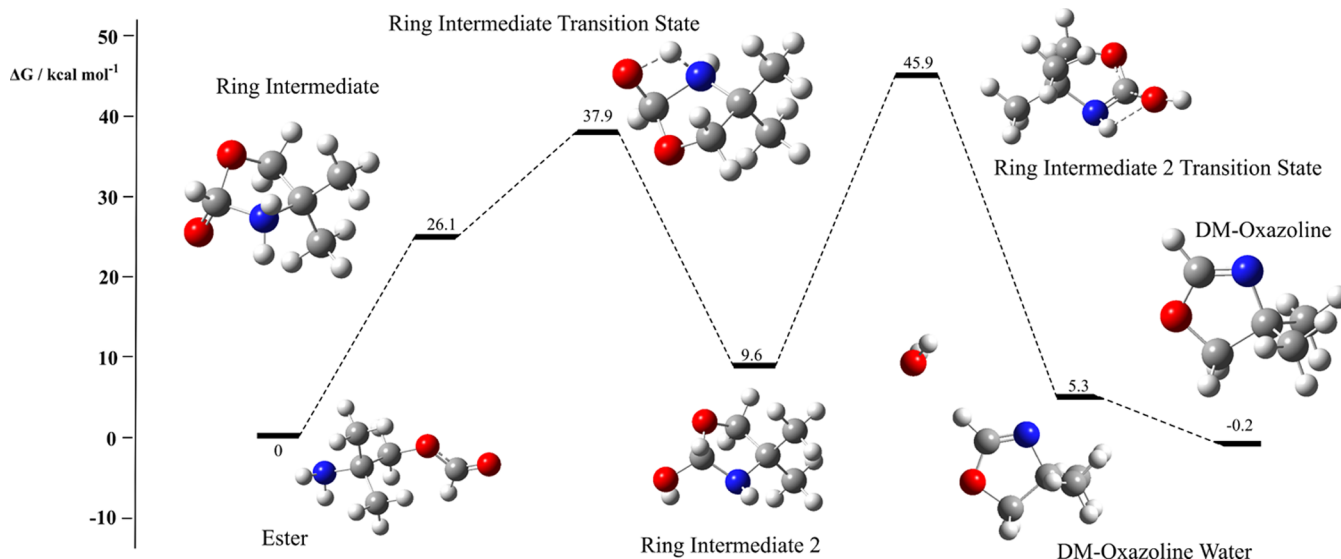


Figure 22. DFT-calculated free-energy profile for the formation of dimethyl-oxazoline from an ester.

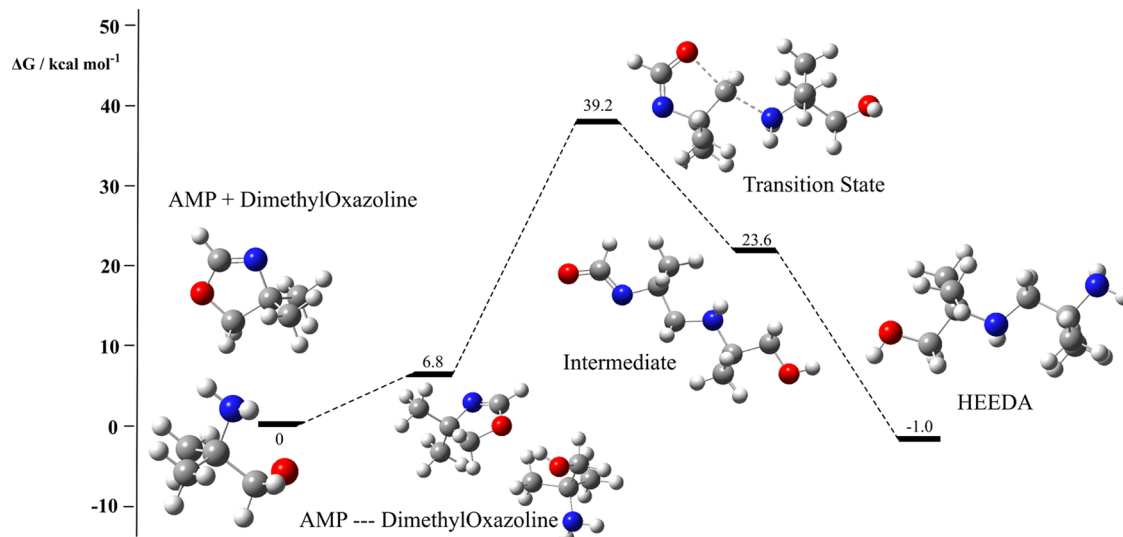


Figure 23. DFT-calculated free-energy profile for the formation of HEEDA from the reaction of AMP and DMOZD.

3.1.6. 2-Methyl-2-(methyleneamino)-1-propanol (DM-MAE) and Imine Formation. The formation of 2-methyl-2-(methyleneamino)-1-propanol (DM-MAE) is analogous to the formation of MAE, which is observed in MEA degradation. It is formed from a condensation reaction of AMP and formaldehyde. The formation of the latter is presented in [Section 3.2.2](#). The reaction is summarized in [Scheme 11](#).

The free-energy profile for this reaction is shown in [Figure 17](#). Initially, AMP acts as a nucleophile and attacks the carbonyl carbon of formaldehyde, leading to a zwitterion (AMP···CH₂O bound in [Figure 17](#)). This species can undergo two subsequent hydrogen transfer reactions to eliminate water and form DM-MAE.

A related reaction can be envisaged where formaldehyde and ammonia can react to form an imine. Comparison of [Figures 17](#) and [18](#) reveals a similar free-energy profile. The nitrogen atom on ammonia initially attacks the carbonyl carbon of formaldehyde. Successive proton transfers yield the target imine. While the free activation energy of the hydrogen transfer step can be lowered by the addition of an explicit water molecule, it is

still appreciably high. This would suggest that the reaction is not overall significant during AMP degradation.

3.1.7. Nitrosamine and Nitramine Formation. The formation of nitrosamines and nitramines during amine-based carbon capture represents a major environmental concern.^{50–52} They are carcinogenic and there are legal limits as to the quantity, which can be vented into the atmosphere. They are formed when nitrogen oxides (NO_x) species react with amines, according to [Scheme 12](#).

Despite multiple attempts, transition states were not located for the reaction of AMP with either NO or NO₂ radicals. Scan calculations along the reaction coordinate showed no discernable saddle point in either case ([Figure S1](#) in the [Supporting Information](#)). Comparison of the energies of the reactants and products suggests that direct reaction of NO and NO₂ with amines is unlikely.

Transition states were located for the reaction of N₂O₃ with AMP. As in [Figure 19](#), this reaction can proceed through a concerted reaction where NO is transferred to the amine nitrogen. Concurrently, a hydrogen is transferred from the

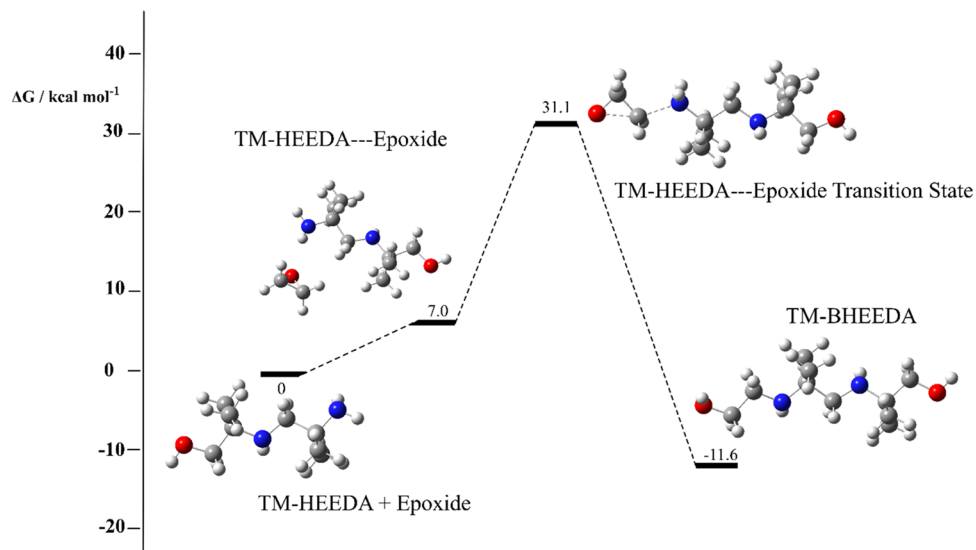


Figure 24. DFT-calculated free-energy profile for the formation of TM-BHEEDA from TM-HEEDA and epoxide.

Scheme 14. Radical Abstraction from Four Unique Sites on AMP

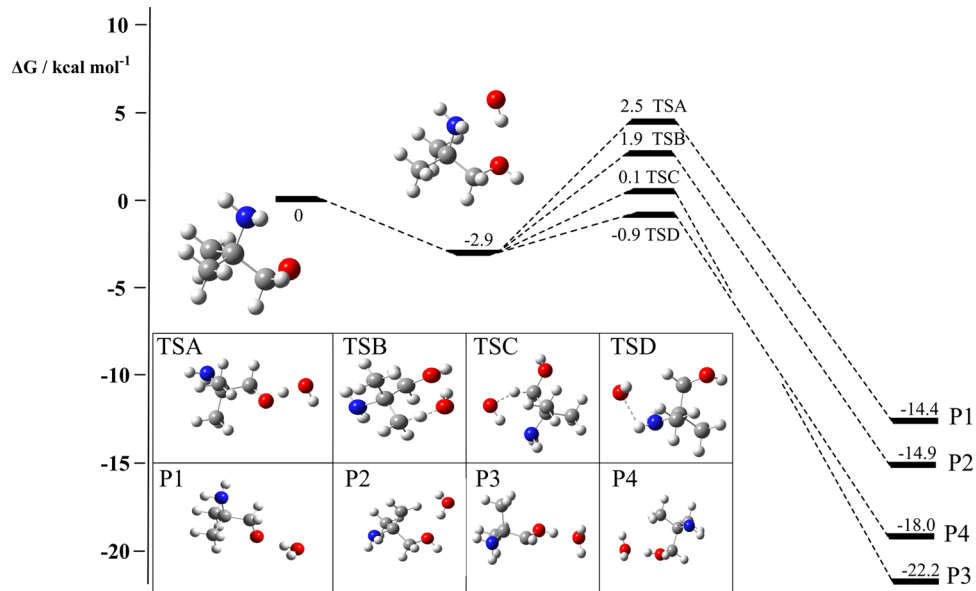
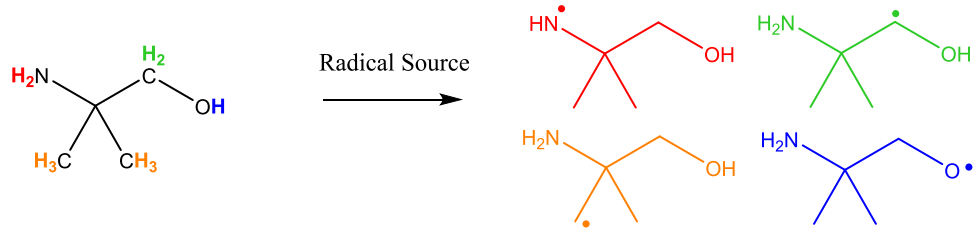


Figure 25. DFT-calculated free-energy profile for radical abstraction from four sites on AMP.

amine to the NO_2 group to form nitric acid. This reaction is predicted to have a relatively low free activation energy (10.6 kcal mol^{-1}), and the reaction is exergonic overall. This would suggest that if any N_2O_3 were present in the reaction system, it would easily react with amines to form nitrosamines.

A similar reaction to that described in Figure 19 could be envisaged for N_2O_4 , which could react with amines through a concerted transition state to form nitramines and HNO_2 . Figure

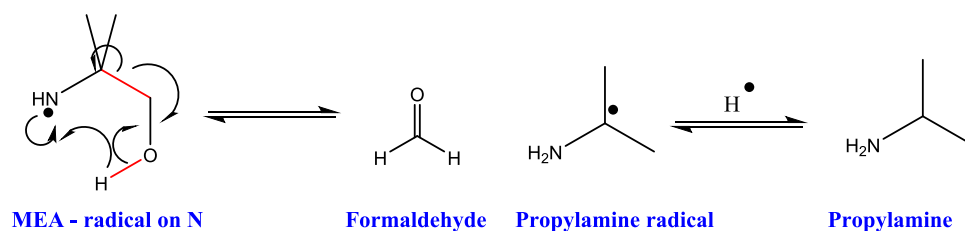
20 shows the free-energy profile for the reaction of N_2O_4 and AMP. The activation free energy is 23.8 kcal mol^{-1} , and the reaction is exergonic overall.

The analyses carried out in Figure 19 for nitrosamine formation and Figure 20 for nitramine formation from AMP was conducted for TM-HEIA, DMOZD, and TM-HEEDA. The results are tabulated in Table 1. As can be seen, free activation energies are larger for both nitrosamine and nitramine formation

Table 2. Free Activation Energies for the Formation of Four Distinct Radicals from AMP after Reaction with Three Different Radicals (Et^\bullet , O_2 , and OH^\bullet)

AMP radical formed	Free activation energy for radical reaction / kcal mol ⁻¹		
	Et^\bullet	OH^\bullet	O_2
	19.6	2.0	39.3
	23.8	3.0	48.5
	19.2	4.8	38.8
	16.9	5.4	46.5

Scheme 15. Potential Fragmentation of an AMP Radical to Form Formaldehyde and a Propylamine Radical^a



^aBonds broken during the reaction are highlighted in red.

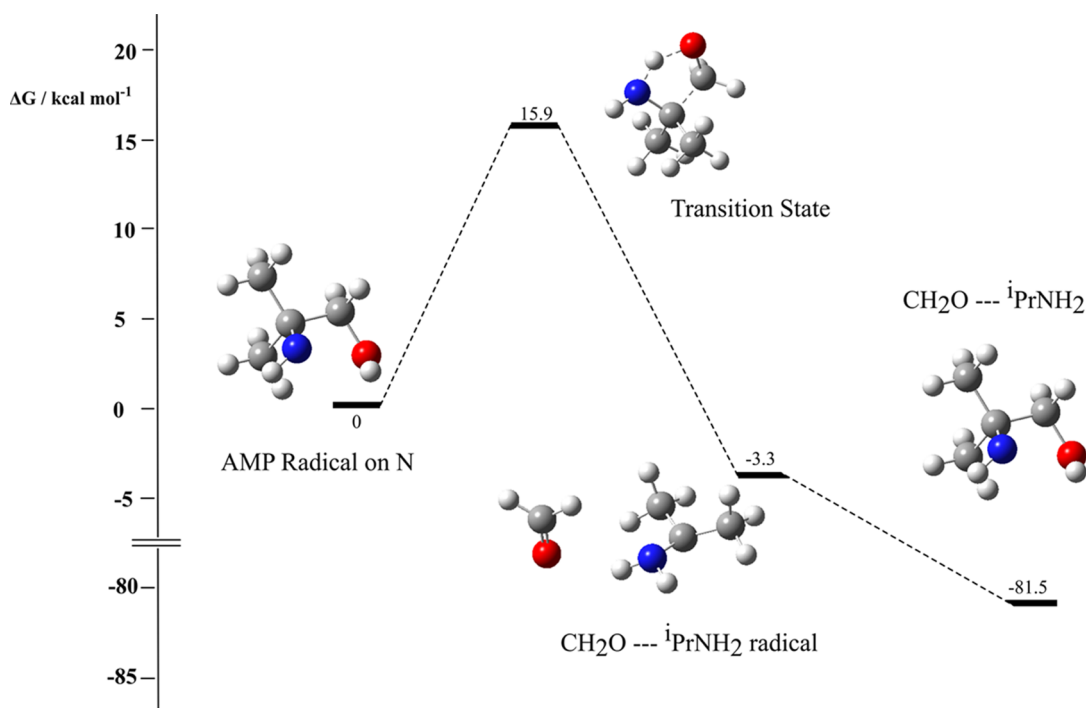
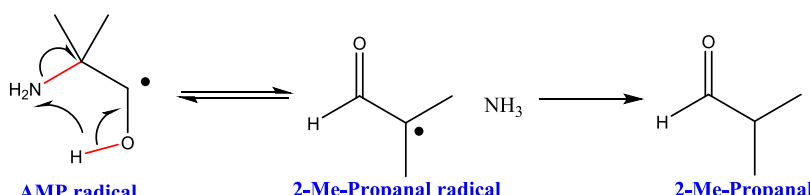
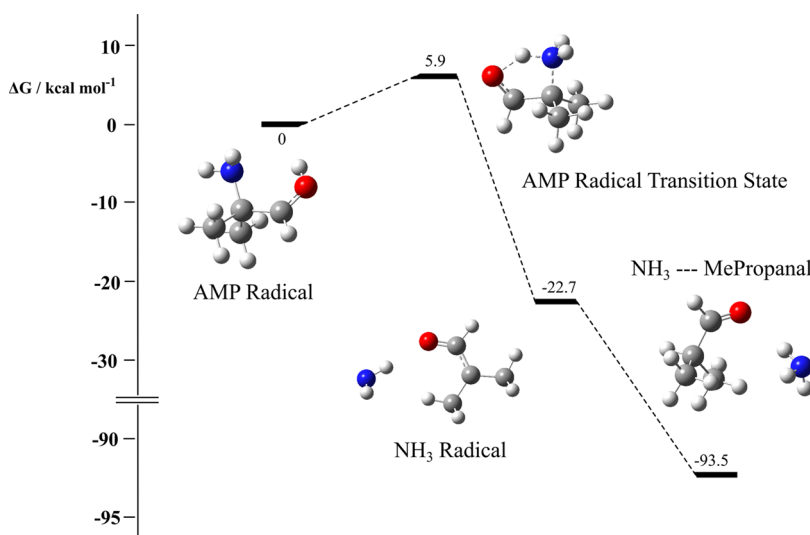


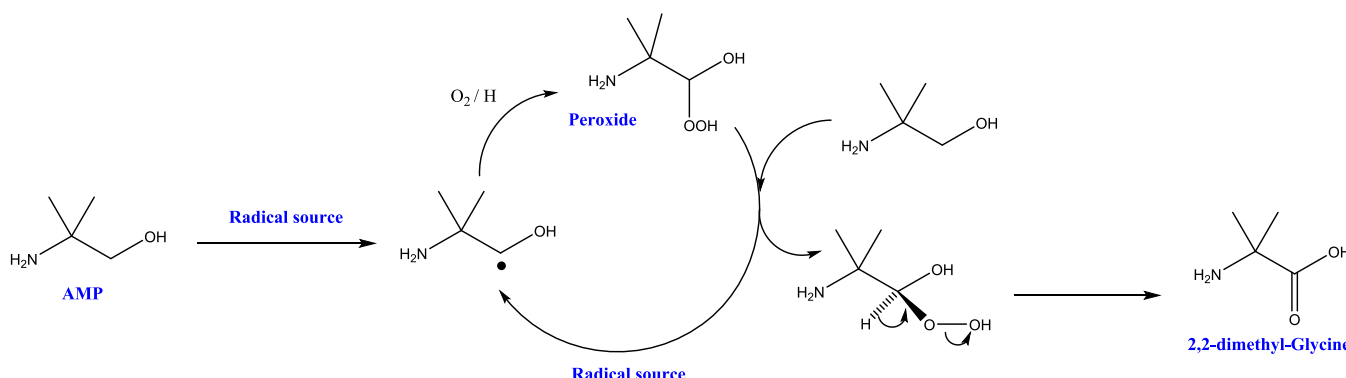
Figure 26. DFT-calculated free-energy profile for radical fragmentation from $\text{HN}\cdot\text{C}(\text{Me})_2\text{CH}_2\text{OH}$.

Scheme 16. Potential Fragmentation of an AMP Radical to Form Ammonia and 2-Me-Propanal Radical^a

^aBonds broken during the reaction are highlighted in red.

Figure 27. DFT-calculated free-energy profile for radical fragmentation from H₂NC(Me)₂C·HOH.

Scheme 17. Potential Route to the Formation of 2,3-Dimethylglycine from AMP



at secondary nitrogen centers than primary centers. Despite this, nitrosamine formation *via* the reaction of amines and N₂O₃ is permissible. In contrast, the formation of nitramines from the reaction of N₂O₄ and amines is less likely due to relatively large activation energies.

3.1.8. TM-HEEDA: An Alternative Route. In Section 3.1.4, we presented a route to the formation of TM-HEEDA *via* a ring-opening reaction between AMP and DMOZD. This reaction had a free activation energy of 40.5 kcal mol⁻¹. An alternative route to the formation of TM-HEEDA is presented here, which is formed through a dimethyl-oxazoline intermediate, as shown in Scheme 13.

Figure 21 shows the DFT-calculated free-energy profile for the formation of an ester from AMP and formic acid. Here, the alcohol group on AMP initially attacks the carbonyl carbon of formic acid. Proton transfer from the cationic oxygen center to

one of the hydroxyl groups leads to the formation of a protonated ester and water. This reaction has a free activation energy of 24.2 kcal mol⁻¹ and a free reaction energy of -22.7 kcal mol⁻¹. While viewed in isolation, this reaction should easily proceed; it will be in competition with the formation of an amide where formic acid is attacked by nitrogen rather than oxygen. This reaction is discussed in more detail in Section 3.2.4.

Once formed, the next step toward the formation of TM-HEEDA is the conversion of the ester into dimethyl-oxazoline. As shown in Figure 22, the nucleophilic attack of the nitrogen atom on the carbonyl carbon leads to the formation of a five-membered ring. A pair of proton transfers, again likely catalyzed by water, leads to the dimethyl-oxazoline product.

The final step is the conversion of dimethyl-oxazoline to TM-HEEDA. This reaction is initiated by a nucleophilic attack of AMP nitrogen on the sp³ carbon of dimethyl-oxazoline. This

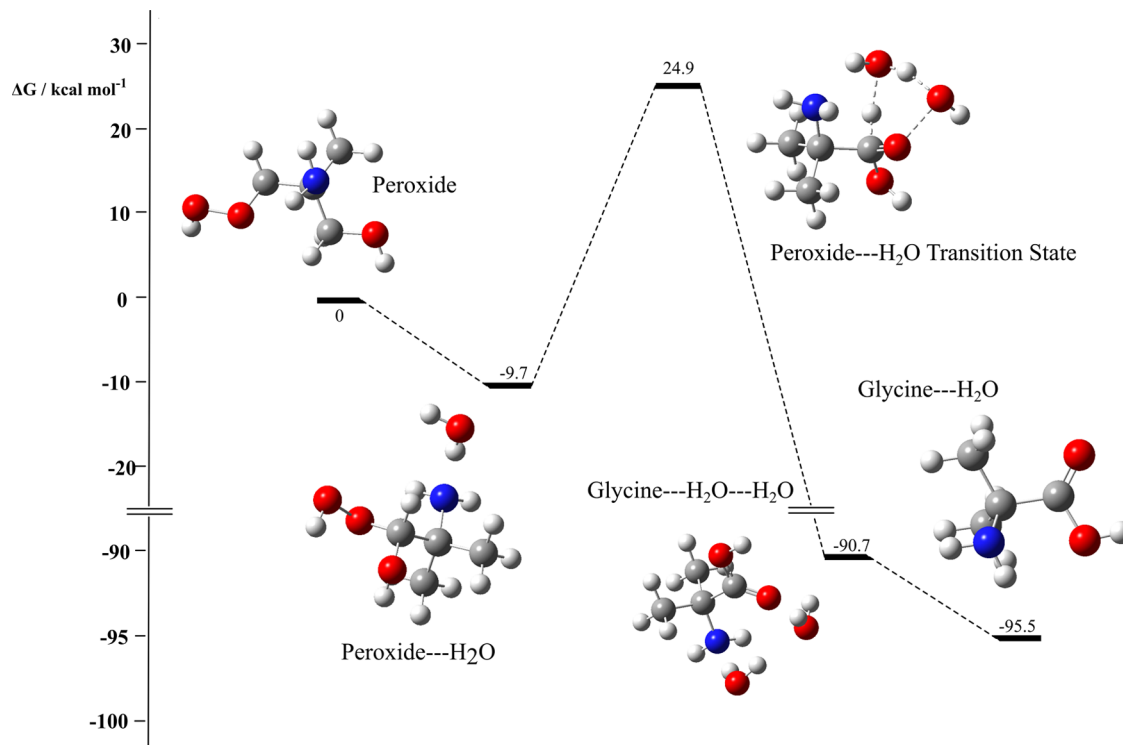


Figure 28. DFT-calculated free-energy profile for the formation of 2,2-dimethylglycine from a peroxide species.

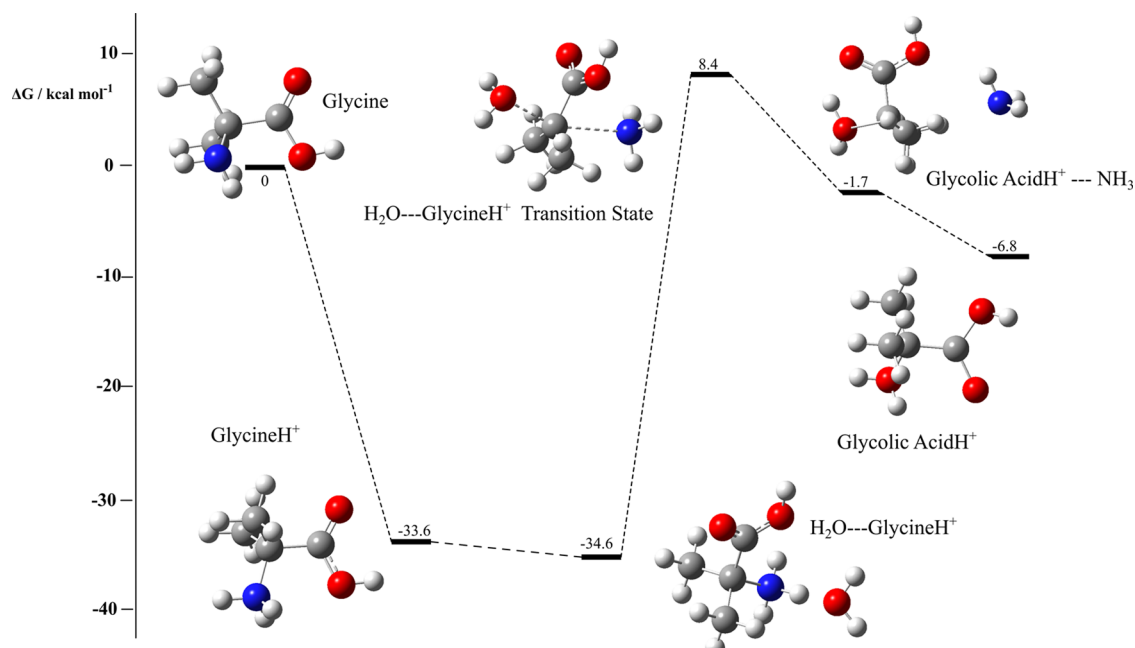


Figure 29. DFT-calculated free-energy profile for the formation of 2,2-dimethylglycolic acid from 2,2-dimethylglycine.

affects a ring-opening reaction and forms a zwitterion intermediate. Rapid hydrogen transfer and hydrolyzation lead to the formation of TM-HEEDA. As shown in Figure 23, this reaction has a free activation energy of 39.2 kcal mol⁻¹.

Overall, while the energy profiles presented in Figures 21–23 demonstrate that TM-HEEDA can be formed *via* an alternative route to that outlined in Section 3.1.3, a series of interconversions and a larger number of molecules are required for this to occur. This route may contribute to some degree to

the TM-HEEDA generated during AMP degradation, but it is unlikely to be the primary route.

Irrespective of the method of formation, TM-HEEDA can undergo a reaction with epoxides (formation of epoxides was proposed in Section 3.1.5) to form N-(2-hydroxyethyl)-N'-(1,1-dimethyl-2-hydroxyethyl)-1,1-dimethylethylenediamine (TM-BHEEDA). The free-energy profile is shown in Figure 24. The reaction energy is overall exergonic and has a surmountable barrier (31.1 kcal mol⁻¹).

Scheme 18. General Scheme for Condensation Reactions to Form Amides

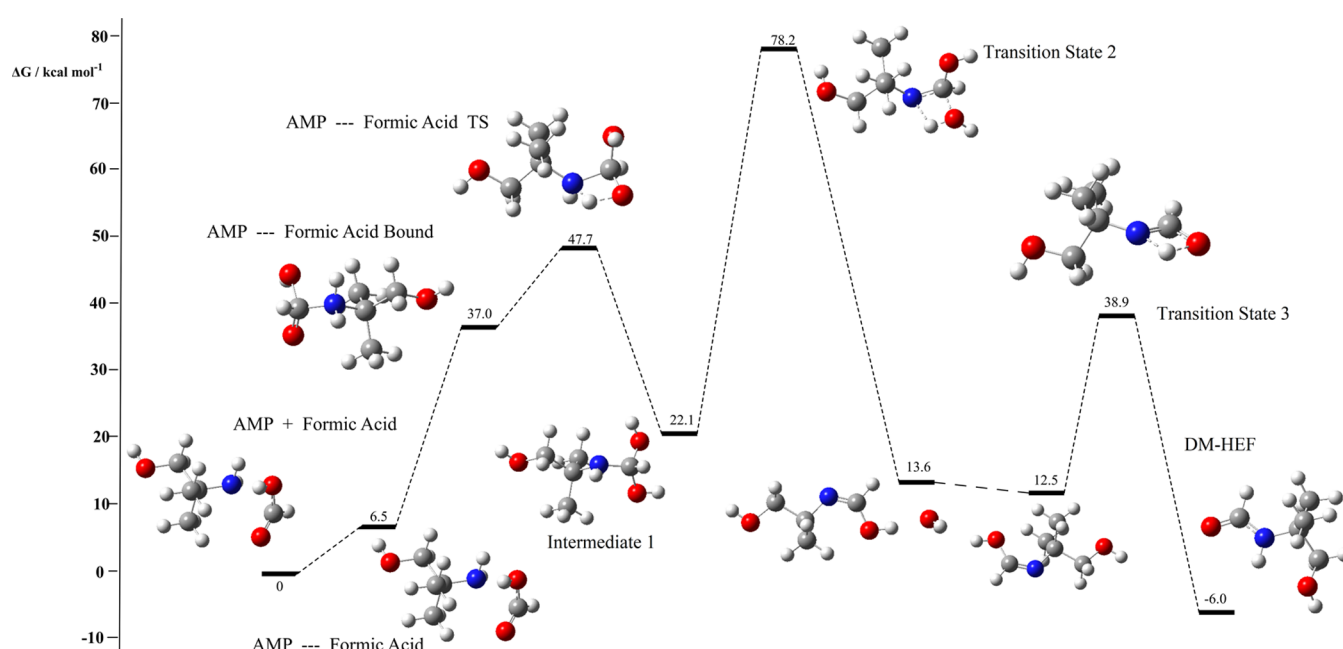
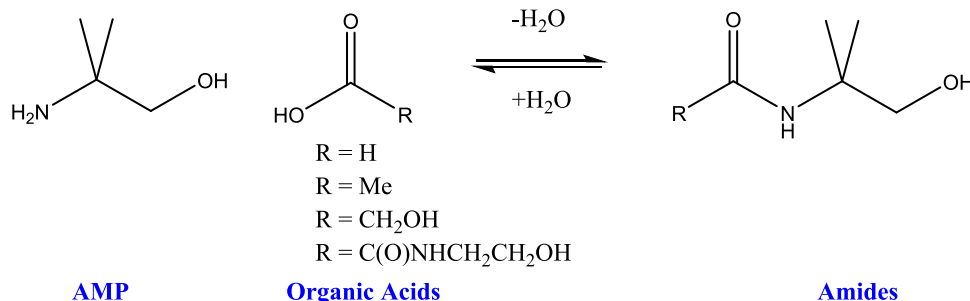


Figure 30. DFT-calculated free-energy profile for the formation of an amide from AMP and formic acid.

Table 3. Free Activation Energies for Amide Formation from the Reaction of AMP and Organic Acids

organic acid R	reaction, kcal mol ⁻¹			
	first hydrogen transfer	second hydrogen transfer	third hydrogen transfer	overall reaction energy
H	47.7	78.2, 42.4 ^a	36.9	-6.0
Me	46.7	83.1	30.0	-4.4
CH ₂ OH	46.7		39.4	-4.2
C(O) NHCH ₂ CH ₂ OH	37.9		36.9	-11.4

^aWater assisted.

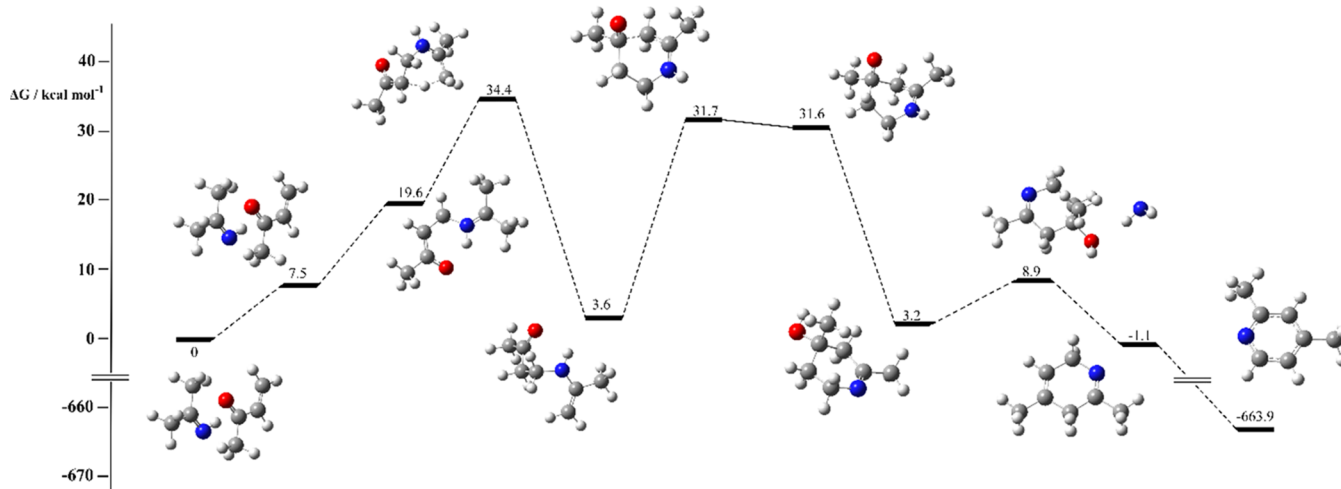
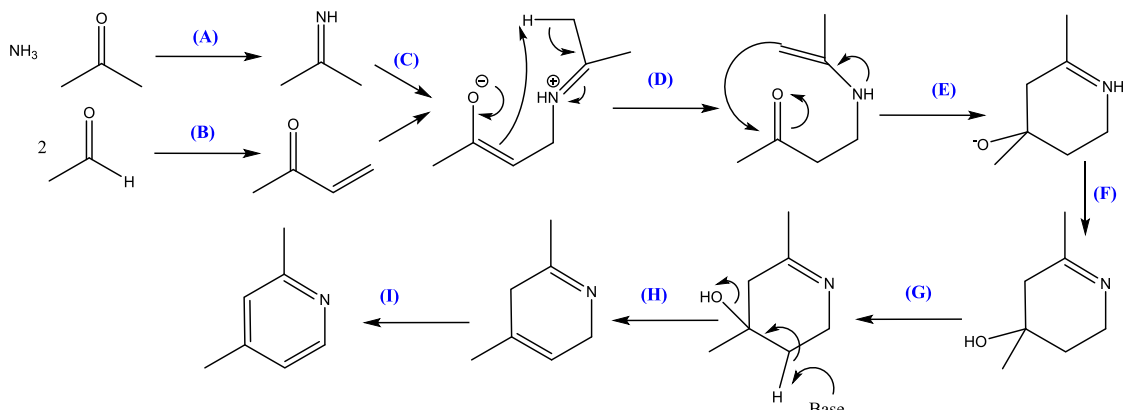
3.2. Oxidative Degradation. The oxidative degradation of amines is considered to be a radical-driven process that occurs mainly in the absorber, where the oxygen concentration is generally higher than in the stripper.^{53–55} The presence of trace metal ions such as Cr³⁺, Fe³⁺, Ni²⁺, and Mn³⁺ are also considered to play a key role in generating radical species. There are a significant number of products, which can result from oxidative degradation. Here, we investigate what are considered to be the main pathways and principal products.

3.2.1. Reactions with OH, Et, and O₂ to Form Radical Species. Oxidative degradation is likely to begin with radical abstraction from amine. As shown in Scheme 14, there are four

sites on AMP where a hydrogen might be abstracted. Namely, the NH₂ group, the pendant methyl groups, the CH₂ linker, and the hydroxy group. The reaction at each of these sites was first investigated using a hydroxyl radical (OH[•]). Figure 25 shows the activation free-energy profile for each reaction. As can be seen, activation free energies are low in all cases, suggesting the facile formation of AMP radicals. The lowest value was calculated for abstraction from the amine with the highest value calculated for abstraction at OH. In each case, reaction free energies are exergonic. Similar results were recently reported for radical abstraction from MEA.³⁸

Each of the reactions in Figure 25 was repeated with both O₂ and Et[•] in place of OH[•]. The collated data is shown in Table 2. The smallest free activation energies are observed for the reactions with OH[•], and reactions with O₂ are predicted to have the largest activation energies.

3.2.2. Radical Fragmentation. Irrespective of the method through which the AMP radical is formed, it can further fragment into smaller species. Scheme 15 shows a potential fragmentation reaction from a radical centered on the amine. A related reaction was first proposed for MEA by Petryaev et al.⁵⁶ and here could lead to the formation of formaldehyde and propylamine. In this reaction, concurrent bond breaking (O—H and C—C) and bond forming (N—H) occur in a single-step reaction.

Scheme 19. Proposed Mechanistic Steps Leading to the Formation of Lutidine from Ammonia, Propanone, and Ethanal**Figure 31.** DFT-calculated free-energy profile for the formation of lutidine.

As can be seen in Figure 26, the reaction is predicted to have a low free activation energy (15.9 kcal mol⁻¹) and radical recombination to form [·]PrNH₂ is strongly exergonic and can help to drive the reaction.

A species with a radical located on the secondary carbon atom can undergo a fragmentation reaction, as shown in Scheme 16. Breaking of the N–C and O–H bonds leads to the formation of ammonia and, initially, a radical that can combine with a hydrogen source to form 2-Me-propanal. Figure 27 shows the free-energy profile for this reaction. As can be seen, the free activation energy is very low (5.9 kcal mol⁻¹) and the reaction energy is strongly exergonic.

3.2.3. Formation of 2,2-Dimethylglycine and 2,2-Dimethylglycolic Acid. The formation of glycine is observed in the experimental degradation studies of MEA, and mechanistic routes to its formation have been proposed by Bedell.^{57,58} Here, we investigated a related reaction beginning with AMP, which can lead to a substituted analogue of glycine, as shown in Scheme 17.

The peroxide species can be formed *via* the reaction of the appropriate AMP radical (*i.e.*, a radical centered on carbon α to oxygen) with oxygen followed by a radical termination step. Once formed, with the addition of a source of base (in this case, AMP), an elimination reaction can occur, which generates 2,2-dimethylglycine. Figure 28 shows that the free activation energy for

for this step is 24.9 kcal mol⁻¹ and the reaction is strongly exergonic overall.

The conversion of 2,2-dimethylglycine into 2,2-glycolic acid occurs through a mechanism similar to that presented for diol formation in Section 3.1.2. The free-energy profile is shown in Figure 29. Prior protonation of glycine forms a structure that is more susceptible to nucleophilic attack and is very favorable. The free activation energy for the hydrolysis reaction is 43.0 kcal mol⁻¹. This is high and thus the formation of glycolic acid is not likely. Moreover, the reaction is endergonic, which suggests that any product formed would likely convert back to the reactants.

3.2.4. Organic Acid Reactions with AMP. A number of organic acids can be formed from radical fragmentation. Any of these can potentially react with AMP to form amides according to Scheme 18. While it is beyond the scope of this work to carry out an exhaustive inquiry into the reactions that can occur, we investigated a few to illustrate what reactions may occur. Figure 30 shows the formation of *N*-(2-hydroxy-1,1-dimethylethyl)-formamide (DM-HEF), which results from the reaction of AMP and formic acid.

Initially, AMP acts as a nucleophile and attacks the carbonyl carbon of formic acid. Subsequent hydrogen transfer from the now cationic nitrogen center forms an intermediate species. This reaction has a free activation energy of 45.7 kcal mol⁻¹. A second hydrogen transfer can occur, which acts to eliminate water and generate an imine intermediate. The free activation energy for

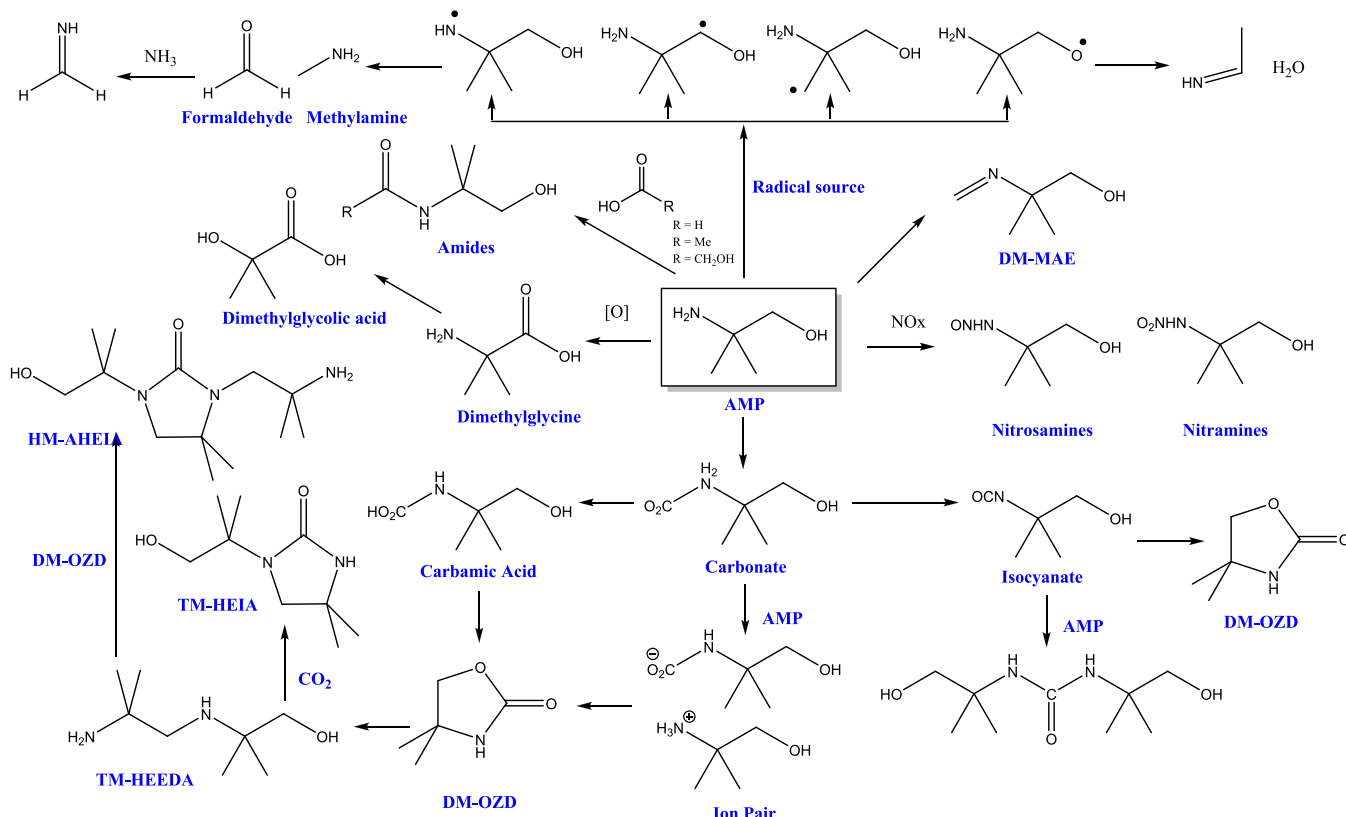


Figure 32. Schematic reaction network detailing the principal interconversions that AMP and its degradation products can undergo.

this conversion is prohibitive at 76.7 kcal mol⁻¹. This value, however, can be significantly reduced with the addition of explicit water. In this case, the free activation energy is 42.4 kcal mol⁻¹. The final step in the formation of an amide is a final hydrogen transfer from the hydroxyl group to the imine nitrogen.

Table 3 details free activation energies for the formation of the remaining amides as postulated in Scheme 18. As can be seen, the activation free energies for each reaction are similar independent of the organic acid. However, given the number of interconversions necessary to reach the products and high free activation energies, it is unlikely that they form in significant quantities. This is supported in experimental studies where they are not observed forming.⁵⁹

3.2.5. 2,4-Lutidine Formation. 2,4-Lutidine is often observed forming in the degradation studies of AMP. The route to its formation, however, is far from trivial. As shown in Scheme 19, a number of reactants are needed to rationalize its formation. Ammonia and propanone combine to form an imine (A) and 2 equiv of ethanal react through an aldol condensation reaction to form 2-butenone (B). The 2-butenone and imine can then react to form 2,4-lutidine.

Initially, the nitrogen on the imine acts as a nucleophile and attacks the terminal carbon of the double bond in 2-butenone (C). This leads to the formation of a zwitterion with a positively charged nitrogen and negatively charged oxygen. The oxygen lone pair can facilitate the reaction of the double bond with a terminal hydrogen (D). The intermediate formed can react to form a six-membered ring (E). Hydrogen transfer from the positively charged nitrogen to the negatively charged oxygen creates a species, which can react with a source of base to eliminate hydroxide. Finally, the penultimate species can be

oxidized to form lutidine (F–I). The free-energy profile for this series of reactions is shown in Figure 31. As can be seen, while there are a number of interconversions necessary to reach the product, free activation energies are surmountable given standard experimental conditions. Moreover, the reaction free energy is strongly exergonic overall, which is expected given that an aromatic ring is being formed.

4. SCHEMATIC REACTION NETWORK

Figure 32 shows a schematic network of all of the elementary reactions investigated here. AMP can react with CO₂ to form either an ion pair or carbamic acid. Both of these species can cyclize to form DMOZD, a substituted variant of OZD. TM-HEEDA can be formed either from DMOZD or via a series of reactions beginning with an esterification. The formation of TM-HEIA and HM-AHEIA is likely to be slow due to large free activation energies.

Radical abstraction from multiple sites on AMP leads to AMP radicals, which can fragment into smaller organic molecules. The formation of amides from the reaction of organic acids with AMP is prohibited by large free activation energies. This is in contrast to MEA systems, where amides readily form.

5. CONCLUSIONS

DFT modeling of the formation of AMP degradation products has been carried out. Computed activation parameters have been compared with experimental observations to rationalize which pathways are likely and which are prohibitive. The major products expected based upon this work are DMOZD, lutidine, and smaller fragmentation products resulting from oxidative degradation. In contrast to observations from MEA degradation, amides resulting from the reaction of AMP and small organic

acids are predicted to be less important due to higher activation energies.

The importance of the specific solvent environment has been highlighted. Activation energies, particularly for hydrogen transfer reactions, are sensitive and better described using an explicit solvent alongside PCM models. This does however come with a considerable computational cost but may be necessary for further improvement of chemical kinetic models.

The work undertaken here has provided a library of elementary reactions for AMP degradation and can be used as the basis of a full chemical kinetic model. Given appropriate experimental data for validation, such a model could be useful in predicting the type and amount of products expected for various experimental setups.

■ ASSOCIATED CONTENT

Supporting Information

The Supporting Information is available free of charge at <https://pubs.acs.org/doi/10.1021/acs.iecr.1c03963>.

Cartesian coordinates for DFT-optimized structures and scan calculations for nitrosamine formation ([PDF](#))

■ AUTHOR INFORMATION

Corresponding Author

Christopher M. Parks – Department of Mechanical Engineering, The University of Sheffield, Sheffield S3 7RD, U.K.; orcid.org/0000-0001-8016-474X; Email: c.m.parks@sheffield.ac.uk

Authors

Kevin J. Hughes – Department of Mechanical Engineering, The University of Sheffield, Sheffield S3 7RD, U.K.

Mohamed Pourkashanian – Department of Mechanical Engineering, The University of Sheffield, Sheffield S3 7RD, U.K.

Complete contact information is available at:

<https://pubs.acs.org/10.1021/acs.iecr.1c03963>

Funding

The work described in this paper was funded by the ACT ALIGN CCUS Project No. 271501. This project received funding from RVO (NL), FZJ/PtJ (DE), Gassnova (NO), UEFISCDI (RO), and BEIS (UK) and was cofunded by the European Commission under the Horizon 2020 programme ACT, Grant Agreement No. 691712.

Notes

The authors declare no competing financial interest.

■ ABBREVIATIONS

AMP	2-amino-2-methyl-1-propanol
AHEIA	<i>N</i> -(2-aminoethyl)- <i>N'</i> -(2-hydroxyethyl)-imidazolidin-2-one
DMOZD	4,4-dimethyl-2-oxazolidinone
HEIA	<i>N</i> -(2-aminoethyl)- <i>N'</i> -(2-hydroxyethyl)-imidazolidin-2-one)
DM-MAE	2-methyl-2-(methyleneamino)-1-propanol
TM-HEEDA	2-[<i>(</i> 2-amino-2-methylpropyl <i>)</i> amino]-2-methyl-1-propanol
HEEDA	<i>N</i> -(2-hydroxethyl)ethylenediamine
OZD	2-oxazolidinone

■ REFERENCES

- (1) Kerr, R. A. Climate change. Global warming is changing the world. *Science* **2007**, *316*, 188–190.
- (2) Rochelle, G. T. Amine Scrubbing for CO₂ Capture. *Science* **2009**, *325*, 1652.
- (3) Rao, A. B.; Rubin, E. S. A Technical, Economic, and Environmental Assessment of Amine-Based CO₂ Capture Technology for Power Plant Greenhouse Gas Control. *Environ. Sci. Technol.* **2002**, *36*, 4467–4475.
- (4) Hsu, C. S.; Kim, C. J. Diethanolamine (DEA) degradation under gas-treating conditions. *Ind. Eng. Chem. Prod. Res. Dev.* **1985**, *24*, 630–635.
- (5) Kennard, M. L.; Meisen, A. Gas chromatographic technique for analysing partially degraded diethanolamine solutions. *J. Chromatogr. A* **1983**, *267*, 373–380.
- (6) Li, J.; Henni, A.; Tontiwachwuthikul, P. Reaction Kinetics of CO₂ in Aqueous Ethylenediamine, Ethyl Ethanolamine, and Diethyl Monoethanolamine Solutions in the Temperature Range of 298–313 K, Using the Stopped-Flow Technique. *Ind. Eng. Chem. Res.* **2007**, *46*, 4426–4434.
- (7) Wang, Z.; Fang, M.; Pan, Y.; Yan, S.; Luo, Z. Amine-based absorbents selection for CO₂ membrane vacuum regeneration technology by combined absorption–desorption analysis. *Chem. Eng. Sci.* **2013**, *93*, 238–249.
- (8) Zhou, S.; Chen, X.; Nguyen, T.; Voice, A. K.; Rochelle, G. T. Aqueous Ethylenediamine for CO₂ Capture. *ChemSusChem* **2010**, *3*, 913–918.
- (9) Chakma, A.; Meisen, A. Identification of methyl diethanolamine degradation products by gas chromatography and gas chromatography–mass spectrometry. *J. Chromatogr. A* **1988**, *457*, 287–297.
- (10) Liu, K.; Jinka, K. M.; Remias, J. E.; Liu, K. Absorption of Carbon Dioxide in Aqueous Morpholine Solutions. *Ind. Eng. Chem. Res.* **2013**, *52*, 15932–15938.
- (11) Mazari, S. A.; Abro, R.; Bhutto, A. W.; Saeed, I. M.; Ali, B. S.; Jan, B. M.; Ghalib, L.; Ahmed, M.; Mubarak, N. M. Thermal degradation kinetics of morpholine for carbon dioxide capture. *J. Environ. Chem. Eng.* **2020**, *8*, No. 103814.
- (12) Ogidi, M. O.; Thompson, W. A.; Maroto-Valer, M. M. Thermal Degradation of Morpholine in CO₂ Post-combustion Capture. *Energy Procedia* **2017**, *114*, 1033–1037.
- (13) Aroonwilas, A.; Veawab, A. Integration of CO₂ capture unit using blended MEA–AMP solution into coal-fired power plants. *Energy Procedia* **2009**, *1*, 4315–4321.
- (14) Brúder, P.; Grimstvedt, A.; Mejell, T.; Svendsen, H. F. CO₂ capture into aqueous solutions of piperazine activated 2-amino-2-methyl-1-propanol. *Chem. Eng. Sci.* **2011**, *66*, 6193–6198.
- (15) Choi, W.-J.; Seo, J.-B.; Jang, S.-Y.; Jung, J.-H.; Oh, K.-J. Removal characteristics of CO₂ using aqueous MEA/AMP solutions in the absorption and regeneration process. *J. Environ. Sci.* **2009**, *21*, 907–913.
- (16) Dash, S. K.; Samanta, A.; Samanta, A. N.; Bandyopadhyay, S. S. Absorption of carbon dioxide in piperazine activated concentrated aqueous 2-amino-2-methyl-1-propanol solvent. *Chem. Eng. Sci.* **2011**, *66*, 3223–3233.
- (17) Mandal, B. P.; Bandyopadhyay, S. S. Absorption of carbon dioxide into aqueous blends of 2-amino-2-methyl-1-propanol and monoethanolamine. *Chem. Eng. Sci.* **2006**, *61*, 5440–5447.
- (18) Xiao, J.; Li, C.-W.; Li, M.-H. Kinetics of absorption of carbon dioxide into aqueous solutions of 2-amino-2-methyl-1-propanol +monoethanolamine. *Chem. Eng. Sci.* **2000**, *55*, 161–175.
- (19) Zhang, P.; Shi, Y.; Wei, J.; Zhao, W.; Ye, Q. Regeneration of 2-amino-2-methyl-1-propanol used for carbon dioxide absorption. *J. Environ. Sci.* **2008**, *20*, 39–44.
- (20) Tontiwachwuthikul, P.; Meisen, A.; Lim, C. J. CO₂ absorption by NaOH, monoethanolamine and 2-amino-2-methyl-1-propanol solutions in a packed column. *Chem. Eng. Sci.* **1992**, *47*, 381–390.
- (21) Hadri, N. E. L.; Quang, D. V.; Abu-Zahra, M. R. M. Study of Novel Solvent for CO₂ Post-combustion Capture. *Energy Procedia* **2015**, *75*, 2268–2286.

- (22) da Silva, E. F.; Lepaumier, H.; Grimstvedt, A.; Vevelstad, S. J.; Einbu, A.; Vernstad, K.; Svendsen, H. F.; Zahlsen, K. Understanding 2-Ethanolamine Degradation in Postcombustion CO₂ Capture. *Ind. Eng. Chem. Res.* **2012**, *51*, 13329–13338.
- (23) Lepaumier, H.; da Silva, E. F.; Einbu, A.; Grimstvedt, A.; Knudsen, J. N.; Zahlsen, K.; Svendsen, H. F. Comparison of MEA degradation in pilot-scale with lab-scale experiments. *Energy Procedia* **2011**, *4*, 1652–1659.
- (24) Moser, P.; Schmidt, S.; Sieder, G.; Garcia, H.; Stoffregen, T. Performance of MEA in a long-term test at the post-combustion capture pilot plant in Niederaussem. *Int. J. Greenhouse Gas Control* **2011**, *5*, 620–627.
- (25) Wang, T.; Jens, K.-J. Towards an understanding of the oxidative degradation pathways of AMP for post-combustion CO₂ capture. *Int. J. Greenhouse Gas Control* **2015**, *37*, 354–361.
- (26) Wang, T.; Jens, K.-J. Oxidative Degradation of Aqueous 2-Amino-2-methyl-1-propanol Solvent for Postcombustion CO₂ Capture. *Ind. Eng. Chem. Res.* **2012**, *51*, 6529–6536.
- (27) Vevelstad, S. J.; Eide-Haugmo, I.; da Silva, E. F.; Svendsen, H. F. Degradation of MEA; a theoretical study. *Energy Procedia* **2011**, *4*, 1608–1615.
- (28) Saeed, I. M.; Lee, V. S.; Mazari, S. A.; Si Ali, B.; Basirun, W. J.; Asghar, A.; Ghalib, L.; Jan, B. M. Thermal degradation of aqueous 2-aminoethylethanolamine in CO₂ capture; identification of degradation products, reaction mechanisms and computational studies. *Chem. Cent. J.* **2017**, *11*, No. 10.
- (29) Yoon, B.; Stowe, H. M.; Hwang, G. S. Molecular mechanisms for thermal degradation of CO₂-loaded aqueous monoethanolamine solution: a first-principles study. *Phys. Chem. Chem. Phys.* **2019**, *21*, 22132–22139.
- (30) Xie, H.-B.; He, N.; Song, Z.; Chen, J.; Li, X. Theoretical Investigation on the Different Reaction Mechanisms of Aqueous 2-Amino-2-methyl-1-propanol and Monoethanolamine with CO₂. *Ind. Eng. Chem. Res.* **2014**, *53*, 3363–3372.
- (31) Matsuzaki, Y.; Yamada, H.; Chowdhury, F. A.; Higashii, T.; Onoda, M. Ab Initio Study of CO₂ Capture Mechanisms in Aqueous Monoethanolamine: Reaction Pathways for the Direct Interconversion of Carbamate and Bicarbonate. *J. Phys. Chem. A* **2013**, *117*, 9274–9281.
- (32) Yamada, H.; Matsuzaki, Y.; Higashii, T.; Kazama, S. Density Functional Theory Study on Carbon Dioxide Absorption into Aqueous Solutions of 2-Amino-2-methyl-1-propanol Using a Continuum Solvation Model. *J. Phys. Chem. A* **2011**, *115*, 3079–3086.
- (33) Yang, X.; Rees, R. J.; Conway, W.; Puxty, G.; Yang, Q.; Winkler, D. A. Computational Modeling and Simulation of CO₂ Capture by Aqueous Amines. *Chem. Rev.* **2017**, *117*, 9524–9593.
- (34) Frisch, M. J.; Trucks, G. W.; Schlegel, H. B.; Scuseria, G. E.; Robb, M. A.; Cheeseman, J. R.; Scalmani, G.; Barone, V.; Mennucci, B.; Petersson, G. A.; Nakatsuji, H.; Caricato, M.; Li, X.; Hratchian, H. P.; Izmaylov, A. F.; Bloino, J.; Zheng, G.; Sonnenberg, J. L.; Hada, M.; Ehara, M.; Toyota, K.; Fukuda, R.; Hasegawa, J.; Ishida, M.; Nakajima, T.; Honda, Y.; Kitao, O.; Nakai, H.; Vreven, T.; Montgomery, J. J. A.; Peralta, J. E.; Ogliaro, F.; Bearpark, M.; Heyd, J. J.; Brothers, E.; Kudin, K. N.; Staroverov, V. N.; Keith, T.; Kobayashi, R.; Normand, J.; Raghavachari, K.; Rendell, A.; Burant, J. C.; Iyengar, S. S.; Tomasi, J.; Cossi, M.; Rega, N.; Millam, J. M.; Klene, M.; Knox, J. E.; Cross, J. B.; Bakken, V.; Adamo, C.; Jaramillo, J.; Gomperts, R.; Stratmann, R. E.; Yazyev, O.; Austin, A. J.; Cammi, R.; Pomelli, C.; Ochterski, J. W.; Martin, R. L.; Morokuma, K.; Zakrzewski, V. G.; Voth, G. A.; Salvador, P.; Dannenberg, J. J.; Dapprich, S.; Daniels, A. D.; Farkas, O.; Foresman, J. B.; Ortiz, J. V.; Cioslowski, J.; Fox, D. J. Gaussian 09, revision D.01; Gaussian, Inc.: Wallingford, CT, 2016.
- (35) Whaley, R. C.; Petitet, A.; Dongarra, J. Automated empirical optimizations of software and the ATLAS project. *Parallel Comput.* **2001**, *27*, 3–35.
- (36) Lee, C.; Yang, W.; Parr, R. G. Development of the Colle-Salvetti correlation-energy formula into a functional of the electron density. *Phys. Rev. B: Condens. Matter Mater. Phys.* **1988**, *37*, 785–789.
- (37) Dunning, T. H., Jr. Gaussian basis sets for use in correlated molecular calculations. I. The atoms boron through neon and hydrogen. *J. Chem. Phys.* **1989**, *90*, 1007–1023.
- (38) Parks, C.; Alborzi, E.; Akram, M.; Pourkashanian, M. DFT Studies on Thermal and Oxidative Degradation of Monoethanolamine. *Ind. Eng. Chem. Res.* **2020**, *59*, 15214–15225.
- (39) Galano, A.; Alvarez-Idaboy, J. R. Kinetics of radical-molecule reactions in aqueous solution: A benchmark study of the performance of density functional methods. *J. Comput. Chem.* **2014**, *35*, 2019–2026.
- (40) Mangiatordi, G. F.; Brémond, E.; Adamo, C. DFT and Proton Transfer Reactions: A Benchmark Study on Structure and Kinetics. *J. Chem. Theory Comput.* **2012**, *8*, 3082–3088.
- (41) Scalmani, G.; Frisch, M. J. Continuous surface charge polarizable continuum models of solvation. I. General formalism. *J. Chem. Phys.* **2010**, *132*, No. 114110.
- (42) Cancès, E.; Mennucci, B.; Tomasi, J. A new integral equation formalism for the polarizable continuum model: Theoretical background and applications to isotropic and anisotropic dielectrics. *J. Chem. Phys.* **1997**, *107*, 3032–3041.
- (43) Funes-Ardoiz, I.; Paton, R. S. GoodVibes, version 2.0.3; Zenodo, 2018.
- (44) Peterson, S. L.; Stucka, S. M.; Dinsmore, C. J. Parallel Synthesis of Ureas and Carbamates from Amines and CO₂ under Mild Conditions. *Org. Lett.* **2010**, *12*, 1340–1343.
- (45) Sakakura, T.; Choi, J.-C.; Yasuda, H. Transformation of Carbon Dioxide. *Chem. Rev.* **2007**, *107*, 2365–2387.
- (46) Yoon, B.; Hwang, G. S. First-Principles Assessment of Anomalous Thermal Degradation of Aqueous 2-Amino-2-methyl-1-propanol for CO₂ Capture. *Energy Fuels* **2021**, *35*, 16705–16712.
- (47) Parks, C.; Hughes, K.; Pourkashanian, M. Rationalizing Product Formation in Piperazine Degradation: A Computational Study. *Ind. Eng. Chem. Res.* **2021**, *60*, 12864–12882.
- (48) Fazio, M. J. Nucleophilic ring opening of 2-oxazolines with amines: a convenient synthesis for unsymmetrically substituted ethylenediamines. *J. Org. Chem.* **1984**, *49*, 4889–4893.
- (49) Lepaumier, H.; Picq, D.; Carrette, P.-L. New Amines for CO₂ Capture. I. Mechanisms of Amine Degradation in the Presence of CO₂. *Ind. Eng. Chem. Res.* **2009**, *48*, 9061–9067.
- (50) da Silva, E. F.; Booth, A. M. Emissions from Postcombustion CO₂ Capture Plants. *Environ. Sci. Technol.* **2013**, *47*, 659–660.
- (51) Karl, M.; Wright, R. F.; Berglen, T. F.; Denby, B. Worst case scenario study to assess the environmental impact of amine emissions from a CO₂ capture plant. *Int. J. Greenhouse Gas Control* **2011**, *5*, 439–447.
- (52) Nielsen, C. J.; Herrmann, H.; Weller, C. Atmospheric chemistry and environmental impact of the use of amines in carbon capture and storage (CCS). *Chem. Soc. Rev.* **2012**, *41*, 6684–6704.
- (53) Fredriksen, S. B.; Jens, K.-J. Oxidative Degradation of Aqueous Amine Solutions of MEA, AMP, MDEA, Pz: A Review. *Energy Procedia* **2013**, *37*, 1770–1777.
- (54) Koppenol, W. H.; Stanbury, D. M.; Bounds, P. L. Electrode potentials of partially reduced oxygen species, from dioxygen to water. *Free Radical Biol. Med.* **2010**, *49*, 317–322.
- (55) Lepaumier, H.; Picq, D.; Carrette, P.-L. New Amines for CO₂ Capture. II. Oxidative Degradation Mechanisms. *Ind. Eng. Chem. Res.* **2009**, *48*, 9068–9075.
- (56) Petryaev, E. P.; Pavlov, A. V.; Shadyro, O. I. Homolytic deamination of amino alcohols. *J. Org. Chem.* **1984**, *20*, 25–29.
- (57) Bedell, S. A. Oxidative degradation mechanisms for amines in flue gas capture. *Energy Procedia* **2009**, *1*, 771–778.
- (58) Bedell, S. A.; Worley, C. M.; Darst, K.; Simmons, K. Thermal and oxidative disproportionation in amine degradation—O₂ stoichiometry and mechanistic implications. *Int. J. Greenhouse Gas Control* **2011**, *5*, 401–404.
- (59) Wang, T.; Jens, K.-J. Oxidative Degradation of AMP/MEA Blends for Post-combustion CO₂ Capture. *Energy Procedia* **2013**, *37*, 306–313.